CrystEngComm

RSC Publishing

PAPER

View Article Online
View Journal | View Issue

Cite this: *CrystEngComm*, 2013, **15**, 6948

Dinuclear Ag(I) metallamacrocycles of bis-*N*-heterocyclic carbenes bridged by calixarene fragments: synthesis, structure and chemosensing behavior†

Cai-Xia Lin,[b] Xiao-Fei Kong,[a] Qing-Shan Li,[a] Zheng-Zhi Zhang,*[a] Yao-Feng Yuan*[b] and Feng-Bo Xu*[a]

Received 24th May 2013,
Accepted 1st July 2013

DOI: 10.1039/c3ce40918j

www.rsc.org/crystengcomm

Dinuclear Ag(I) metallamacrocycles containing bis-*N*-heterocyclic carbene units and calixarene fragments [{1,1′-R^2-3,3′-CH_2{(*p*-R^1-$C_6H_2OMe)CH_2$}$_m$-bisimidazol-2-ylidene}$_2$-Ag_2]$(PF_6)_2$ (**6a–f**), (**6a**: m = 1, R^1 = Me, R^2 = Me; **6b**: m = 1, R^1 = *t*-Bu, R^2 = Me; **6c**: m = 1, R^1 = Me, R^2 = naphthylmethyl; **6d**: m = 1, R^1 = Me, R^2 = anthrylmethyl; **6e**: m = 2, R^1 = Me, R^2 = anthrylmethyl; **6f**: m = 3, R^1 = *t*-Bu, R^2 = anthrylmethyl) were synthesized by reacting silver oxide with the corresponding bis-imidazolium salts (**5a–f**). Single crystal structural analyses reveal that metallamacrocycles of diverse sizes consisting of two NHC–Ag(I)–NHC units and two calixarene fragments are found in the structures of these dinuclear complexes. These complexes show different configurations with the change of the upper-rims (R^1) of the calixarene fragments or *N*-substituents (R^2) of the NHC rings. The two bis-NHC ligands in the complexes generally adopt *trans*-conformations except for the pair in **6b**. Complexes **6a** and **6c–d**, in which R^1 are methyl groups, show rectangular cavities in their structures. Complex **6b**, in which R^1 are *tert*-butyl groups of great steric hindrance, adopts cone conformation analogous to that of the calixarene. Interestingly, cation–π interactions are present between Ag(I) and the π–electron rich arene ring of R^2 in the structures of complexes **6c–f**. Intermolecular C–H···F hydrogen bonds exist in the crystal packing of all these complexes. Moreover, intermolecular Ag···Ag interactions are found in complex **6a** and intermolecular π–π interactions are observed in complexes **6c–f**. These intermolecular interactions lead to the formation of 2D supramolecular layers in complex **6c** and 3D supramolecular networks in complexes **6a–b** and **6d–f**, respectively. The fluorescent chemosensing behaviors of these metallamacrocycles were explored for some neutral molecules. The results showed that **6d** can behave as an efficient fluorescent chemosensor for *p*-benzoquinone and **6e–f** exhibit fluorescent quenching behaviors for C_{60} or C_{70} fullerenes.

Introduction

N-Heterocyclic carbenes (NHC) are weak π-acceptors and strong σ-donors and can form strong M–C bonds with transition metal centers.[1] Due to the high stability of M–C NHC-bonds, NHC metal complexes exhibit unusual chemical and physical properties and have received a great deal of interest for many years.[2] NHC metal complexes are widely used in the field of catalysis,[3] medicine,[4] luminescent components,[5] functional materials[6] and supramolecular chemistry.[7] In recent years, lots of dinuclear bis-NHC metal complexes bridged by alkyl,[8] aryl[9] or ether chains[10] have been studied and some of them displayed novel structures[4b,8e,9g] and showed promising applications in catalysis,[9d,10b] luminescence[11] and medicine chemistry.[9c,9e,12] What we are interested in is to design and synthesize dinuclear macrocyclic NHC metal complexes which can be applied as host molecules in supramolecular chemistry to recognize neutral organic molecules *via* multiple sites.[9b] As is known, calixarenes are a class of important and versatile host molecules because of their unique conformational and special cavity structures.[13] Some attempts have been made to prepare metal NHC–calixarene complexes by attaching NHC–metal substituents at the upper/

[a]*State Key Laboratory and Institute of Elemento-Organic Chemistry, Nankai University, Tianjin 300071, P. R. China. E-mail: zzzhang@nankai.edu.cn; xufb@nankai.edu.cn; Fax: +86-22-23503710; Tel: +86-22-23503710*
[b]*Department of Chemistry, Fuzhou University, Fuzhou 350108, P. R. China. E-mail: yaofeng_yuan@fzu.edu.cn*

† Electronic supplementary information (ESI) available: C–H···F hydrogen-bonds and intermolecular π–π interactions of **6a–f** are summarized in Tables S1 and S2. ^{1}H NMR spectra of compounds **5a–f** and **6a–f** are given in Fig. S1–S14. DOSY-NMR spectrum of complex **6d** is given in Fig. S15. TGA, DSC and variation temperature ^{1}H NMR spectrum of complex **6c** are given in Fig. S16 and S17. The determination of the association constants of **6d** and BQ are given in Fig. S18. ^{1}H NMR spectrum of **6d** and the BQ mixture in DMSO-d_6 is given in Fig. S19. Fluorescence titration spectra of **6e** and **6f** to fullerenes are given in Fig. S20–S23. Crystallographic information files in CIF format, CCDC 898036, 906066, 898037, 898043, 931824 and 930716 for complexes **6a–f**, respectively. For ESI and crystallographic data in CIF or other electronic format see DOI: 10.1039/c3ce40918j

lower rims of calixarene in the literature.[14] Our strategy is to synthesize dinuclear macrocyclic bis-NHC Ag(I) complexes using calixarene fragments as linkers. These complexes are assembled *via* M–C bonds of high stability and these kinds of macrocyclic complexes could be defined as a type of calixarene analogue with a rigid metal-framework and flexible aryl chains. In addition, luminescent properties can be easily introduced to this system by attaching fluorophores to the N-atom of the NHC rings. Two metallamacrocycles of this kind have been prepared in our laboratory and one of them with an anthracene fluorophore $[(\mathbf{BIMAn})_2Ag_2](PF_6)_2$ [**BIMAn** = bis{3-(*N*-9-anthrylmethyl-imidazol-2-ylidene)methyl-5-*tert*-butyl-2-methoxyphenyl}methane] behaved as an efficient fluorescent chemosensor for C_{60} fullerene.[15] Here, we report the continuous studies on the synthesis and characterizations of this series of dinuclear macrocyclic bis-NHC Ag(I) complexes $[\{1,1'\text{-}R^2\text{-}3,3'\text{-}CH_2\text{-}\{(p\text{-}R^1\text{-}C_6H_2OMe)CH_2\}_m\text{-bisimdiazol-2-ylidene}\}_2Ag_2](PF_6)_2$ (**6a–f**), (**6a**: $m = 1$, R^1 = Me, R^2 = Me; **6b**: $m = 1$, R^1 = *t*-Bu, R^2 = Me; **6c**: $m = 1$, R^1 = Me, R^2 = naphthylmethyl; **6d**: $m = 1$, R^1 = Me, R^2 = anthrylmethyl; **6e**: $m = 2$, R^1 = Me, R^2 = anthrylmethyl; **6f**: $m = 3$, R^1 = *t*-Bu, R^2 = anthrylmethyl).

Results and discussion

Synthesis of dinuclear Ag(I) complexes 6a–f

The general synthesis of complexes **6a–f** is illustrated in Scheme 1. The bisalcohols of calixarene fragment **1** were applied as starting materials. After sequential methylation and bromination from **1**, the corresponding dibromides **3** were prepared.[16] Treatments of the bromides **3** with *N*-substituted imidazoles **4** in refluxing 1,4-dioxane gave the corresponding bisimidazolium bromides as white solids precipitated from the reaction solutions. The bisimidazolium bromides were converted to **5a–f** by anionic exchange with NH_4PF_6 in methanol as hexafluorophosphate counteranions are usually favorable for the preparation of a dinuclear bi-NHC Ag(I) complex.[4b,9a,17] Dinuclear NHC–Ag(I) complexes **6a–f** were afforded in 70–82% isolated yields by the reaction of bis-NHC precursors **5a–f** with 2.0 mole eq. silver oxide in acetonitrile at 50 °C overnight.

In the ^{1}H NMR spectra of precursors **5a–f**, the characteristic resonances for the C2–H imidazolium acidic protons appear at 9.0–9.4 ppm and the ^{13}C NMR signals are displayed at 134.8–136.8 ppm, which are consistent with those of the reported imidazolium salts.[18] Meanwhile, the ^{1}H NMR spectra of complexes **6a–f** showed the disappearance of the characteristic resonances for the acidic protons in **5a–f**, which confirmed the formation of NHC–Ag(I) complexes.

In the ^{1}H NMR spectra of **6a** and **6b**, the proton signals, except those for C2–H, are similar in their chemical shifts to those of the corresponding groups in precursors **5a** and **5b**. (Table 1 and Fig. S1–S4, ESI†). However, on comparing the ^{1}H NMR spectra of **6c–f** to those of **5c–f** respectively, significant upfield shifts of the corresponding groups were observed. The upfield shift effects can be attributed to the shielding effects of

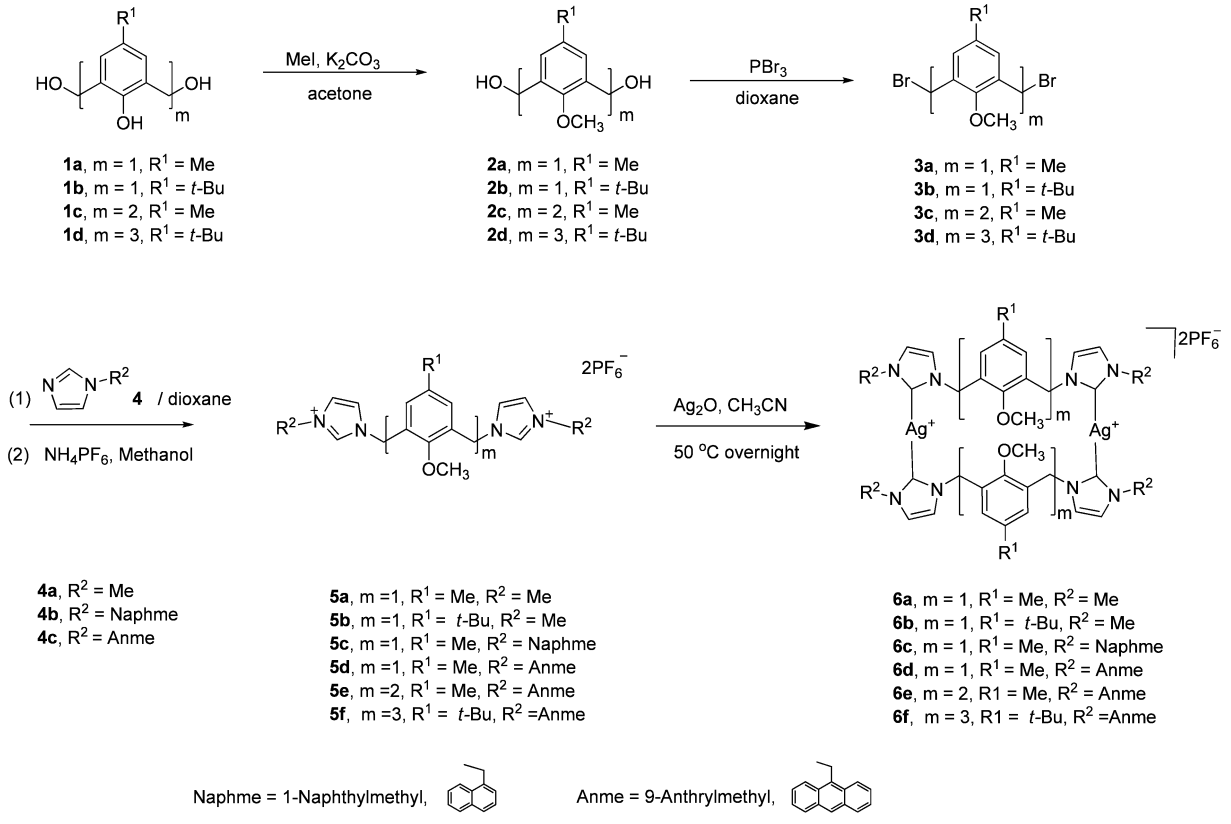

Scheme 1 Synthesis of complexes **6a–f**.

Table 1 Comparison of the NMR chemical shifts (ppm) between complexes **6a–f** and the corresponding precursors **5a–f** (d_6-DMSO, 298 K)

	^{1}H NMR δ (ppm)					^{13}C NMR δ (ppm)				
	Ph–H[a]	Im–CH_2–Ph[b]	Im–CH_2–An[c]	–OCH_3[d]	R^1–H[e]	NCN[f]	Im–CH_2–Ph	Im–CH_2–An	–OCH_3	R^1–C
5a	7.16	5.41	—	3.76	2.26	136.8	47.3	—	62.1	20.3
6a	6.77	5.21	—	3.56	2.04	179.4	47.9	—	60.4	19.2
5b	7.47	5.42	—	3.76	1.26	136.7	47.7	—	62.0	30.9
6b	7.08	5.23	—	3.52	1.09	179.4	48.8	—	60.4	29.7
5c	7.01	5.40	5.94	3.60	2.19	136.8	47.3	50.1	61.8	20.3
6c	6.26	4.85	5.64	3.02	1.75	179.8	48.2	51.0	59.9	19.1
5d	6.83	5.28	6.51	3.40	2.12	136.2	45.0	47.3	61.5	20.3
6d	5.28	4.15	6.05	2.29	1.08	181.0	46.0	48.8	60.0	19.7
5e	6.74[g]	5.30	6.53	3.44	2.09	136.2	45.0	47.9	60.9	20.4
6e	6.10, 5.88[g]	4.16	6.04	2.50	1.60	180.9, 179.0	46.0	50.0	59.9	20.0
5f	7.01, 6.95, 6.92[h]	5.35	6.55	3.51, 3.44[i]	1.07[j]	134.8	43.9	47.1	59.2[i]	29.9, 29.8[j]
6f	6.59, 6.48, 5.87[h]	4.11	6.11	3.14, 2.54[i]	0.98, 0.43[j]	180.5, 178.5	45.9	49.7	60.3, 60.1[i]	31.0, 30.3[j]

[a] Ph refers to the benzene rings in the compounds. [b] Im refers to the imidazolium rings in **5a–f** or the NHC rings in **6a–f**. [c] An refers to the arene rings of R^2 in compounds **5c–d** and **6c–d**. [d] OCH_3 refers to the methoxy groups substituted on the benzene rings in the compounds. [e] R^1 refers to the methyl or *tert*-butyl groups substituted on the benzene rings in compounds **5a–f** and **6a–f**. [f] Carbons at the C2-position of the imidazolium in compounds **5a–f** or carbene-C in compounds **6a–f**. [g] Protons of the benzene rings in **5e** become magnetically nonequivalent in complex **6e**. [h] Three groups of magnetically nonequivalent protons of the benzene rings in **5f** and **6f**. [i] Methoxy groups of the benzene rings in **5f** and **6f** and the methoxy group close to the anthracene rings are magnetically nonequivalent to the methoxy far to anthracene rings. [j] *Tert*-butyl groups of the benzene rings in **5f** and **6f** and the *tert*-butyl groups close to the anthracene rings are magnetically nonequivalent to the *tert*-butyl groups far from the anthracene rings in **6f**.

the naphthalene or anthracene rings in the R^2 groups attached to the NHC rings of **6c–f**. For example, on comparing the ^{1}H NMR spectra of complex **6d** to **5d**, the significant shifts are found as follows: the signals for the benzene ring protons shifted from 6.83 to 5.28 ppm, the signals for the methylene groups between the NHC rings and benzene rings shifted from 5.28 to 4.15 ppm, the signals for the methoxy groups of the benzene rings shifted from 3.40 to 2.29 ppm and the signals for the methyl groups of the benzene rings shifted from 2.02 to 1.08 ppm, respectively. In the ^{1}H NMR spectrum of complex **6f**, the signals for the four protons on the benzene rings close to the anthracene rings shifted upfield from 7.02 to 5.87 ppm, the signals for the methylene groups between the NHC rings and benzene rings shifted from 5.35 to 4.11 ppm, the signals for the four methoxy groups adjacent to the anthracene rings shifted from 3.51 to 2.54 ppm and the signals for the four *tert*-butyl groups of the benzene rings close to the anthracene rings shifted from 1.05 to 0.43 ppm (Fig. S13 and S14, ESI†), respectively. The carbene carbon peaks of complexes **6a–d** appeared as a singlet at 179.4, 179.4, 179.8 and 181.1 ppm, respectively. To be noted, in the ^{13}C NMR spectra of complexes **6e–f**, the signals of the carbene carbons appeared as two doublets at the range of 178.2–181.0 ppm, coupled by silver isotopes ($^1J(^{13}C–^{107}Ag)$ = 183.1 Hz, $^1J(^{13}C–^{109}Ag)$ = 212.5 Hz for complex **6e** and $^1J(^{13}C–^{107}Ag)$ = 184.0 Hz, $^1J(^{13}C–^{109}Ag)$ = 212.4 Hz for complex **6f**).[17,19]

Additionally, the reaction solution of **5d** with Ag_2O was subject to a DOSY-NMR experiment (Fig. S15, ESI†) to detect the other formed products in the reaction. The ^{1}H NMR of the solution clearly showed the characteristic peaks of complex **6d** in above 90% peak strength and the other peaks, corresponding to the by-products, appeared at less than 10%. According to Stokes–Einstein equation,[20] the mean diffusion coefficient of the peaks corresponding to **6d** is 1.019×10^{-10} m^2 s^{-1} (Table S3, ESI†), giving a rough particle radii of complex **6d** of 10.78 Å, which is in agreement with the Ag···Ag distance of 8.859 Å, obtained from the single-crystal data for **6d** (Table 2). Since the other peaks did not give an identical diffusion coefficient, other by-product particles, such as metal–ligand complexes of $[M_1L_1]$ or $[M_3L_3]$, cannot be detected from the DOSY-NMR experiments.

These complexes are stable in their solid form and in solution. The thermogravimetric (TG) and differential scanning calorimetry (DSC) analyses of complex **6c** were representatively performed to investigate the stability of this macrocycle in its solid form. The TG and DSC curve (Fig. S16, ESI†) of complex **6c** showed an initial loss of 0.9% of the crystallized solvents before the decomposition of the complex at about 285 °C, implying the high stability of the dinuclear Ag(I)–NHC macrocycles as a solid.[21] A significant weight loss of *ca.* 55.9% between 285–600 °C is assigned to the decomposition of the complex. In addition, the ^{1}H NMR spectra of **6c** with the temperature varying from 293 K to 353 K showed little change, implying these macrocyclic complexes are stable in solution (Fig. S17, ESI†).

Crystal structures and characterizations of complexes 6a−f

To confirm the molecular structures of the prepared dinuclear macrocyclic complexes, single crystals of **6a–f** were grown and the structures were determined by X-ray diffraction analysis. The structural descriptions of complexes **6a–f** are summarized in Fig. 1 and Table 2. As can be seen in Fig. 2a–7a, large cavities consisting of two NHC–Ag(I)–NHC units and two calixarene fragments can be observed in the structures of **6a–f**,

Table 2 Structural descriptions of complexes **6a–f** according to their X-ray structure analysis

	Space group	Intramolecular Ag···Ag/Å	δAg(C_4)[a]/Å	φ[b]/°	β[c]/°	δ_2[d]/Å	θ_1[e]/°	θ_2[f]/°
6a	*Ibam*	6.792	0.0004	42.34	0	0	33.65	33.65
6b	*P*2(1)/*n*	6.841	Ag1, 0.058, Ag2, 0.046	39.97, 28.64	68.570	—	40.99, 49.82	5.52, 4.84
6c	$P\bar{1}$	9.235	0.032	77.24	0	4.927	74.02	74.02
6d	*C*2/*c*	8.859	0.021	82.44	0	5.071	86.72	86.72
6e	$P\bar{1}$	12.546	Ag1, 0.096, Ag2, 0.118	66.99, 63.38; 22.15, 7.93	8.255 (A, A′)[g], 14.197 (B, B′)	—	68.44, 82.07	83.59, 67.18
6f	$P\bar{1}$	16.986	0.013	63.43, 41.62, 73.19	0, (A, A′)[h], 0, (B, B′), 0 (C, C′)	8.184[h], 8.900, 3.758	80.21	80.21

[a] δAg(C_4) are the deviations of the relevant silver atoms from the plane of the four carbene carbons. [b] φ are the dihedral angles from the plane of the benzene rings to the (carbene-C)$_4$ plane. [c] β are the dihedral angles between two intramolecular benzene rings. [d] δ_2 are the face-to-face distances of two intramolecular benzene rings. [e] θ_1 are the dihedral angles between the pair of NHC rings within a ligand. [f] θ_2 are the dihedral angles between the pair of NHC rings in the same NHC–Ag–NHC unit. [g] β and δ_2 of complex **6e** are relative to two pairs of benzene rings (A, A′) and (B, B′) in an *anti*-conformation (see Fig. 1, **6e**). [h] β and δ_2 of complex **6f** are relative to three pairs of benzene rings (A, A′) (B, B′) and (C, C′) in an *anti*-conformation (see Fig. 1, **6f**).

and the two bis-NHC ligands in the complexes generally adopt *trans*-conformations, except for the pair in **6b**. The Ag–C bond distances are different, in the range of 2.074 Å to 2.095 Å, and all the silver(I) atoms in the complexes have nearly a linear coordination geometry, with the C–Ag–C bond angles ranging from 173.5° to 179.2°, which are similar to the values reported for Ag(I)–NHC complexes.[4b,17] Moreover, in complexes **6a–f**, two NHC–Ag(I)–NHC axes are in mutually parallel positions and the Ag to Ag separations vary from 6.792 Å to 16.986 Å. With the change of the upper-rims of the calixarene fragments (R^1) or *N*-substituents of the NHC rings (R^2), the configurations of the complexes are different.

Complex **6a** crystallizes in a highly symmetric *Ibam* space group. As shown in Fig. 2a, two bis-NHC ligands in the complex adopt a *trans*-conformation. The intramolecular Ag to Ag distance is 6.792 Å. Two benzene rings are coplanar and outwards from the mean plane of the four carbene carbon donors (δAg(C_4) = 0.0004)[22] in opposite directions and the dihedral angle (φ) between the plane of the benzene ring and the (carbene-C)$_4$ plane is 42.34°. Two NHC rings within a ligand form dihedral angles of 33.65° and point to the same side of the (carbene-C)$_4$ plane. Two NHC rings coordinated to the same silver(I) ion are arranged in opposite dispositions according to the (carbene-C)$_4$ plane. In contrast, owing to the disordered properties of the *tert*-butyl groups and hexafluorophosphate, complex **6b** crystallizes in the *P*2(1)/*n* space group of low symmetry. Compared with **6a**, two bis-NHC ligands in **6b** adopt a *trans*-conformation and the two intramolecular benzene rings are no longer coplanar but form a dihedral angle (β) of 68.570° because of the steric hindrance of the *tert*-

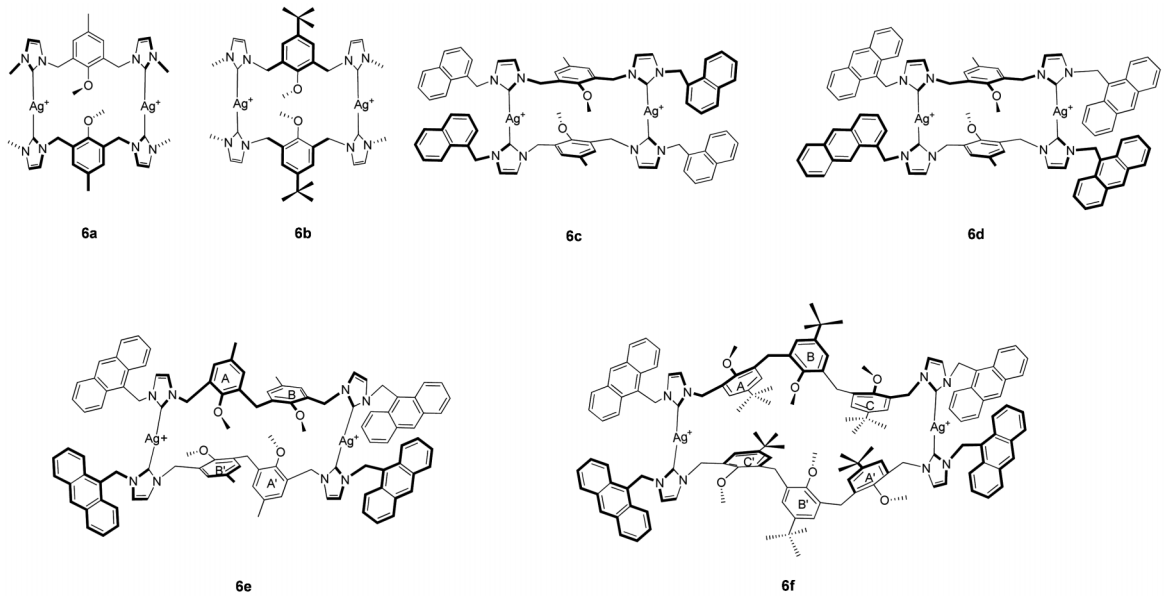

Fig. 1 Illustration of the molecular structures of the complexes.

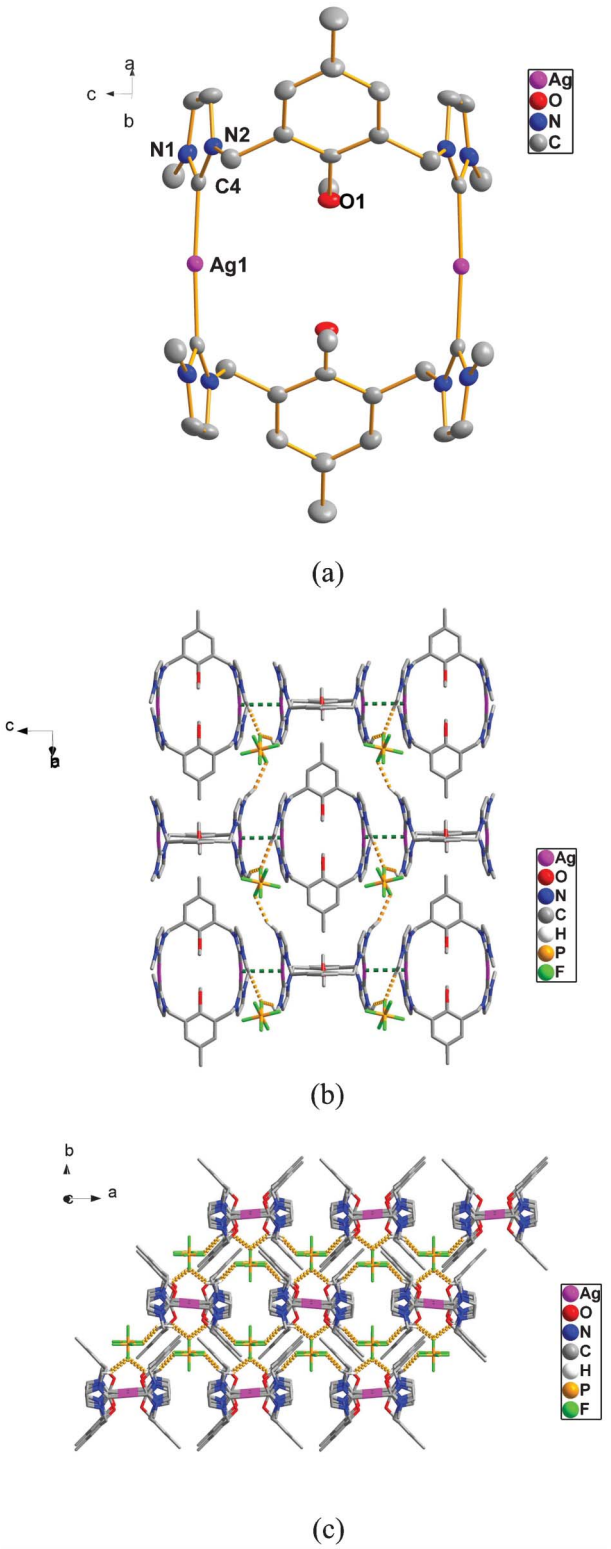

Fig. 2 (a) Molecular structure of complex **6a** (50% probability ellipsoids), hydrogen atoms and anions have been omitted for clarity. Selected bond lengths (Å) and angles (°): Ag1–C4 = 2.088(3); C4–Ag1–C4A = 175.98(13); N1–C4–N2 = 104.5(2). (b) The 2D supramolecular layer of complex **6a** *via* intermolecular Ag···Ag interactions and C–H···F hydrogen bonds. The irrelevant hydrogen atoms have been omitted for clarity. (c) The 3D supramolecular architecture of complex **6a** *via* intermolecular Ag···Ag interactions and C–H···F hydrogen bonds. The irrelevant hydrogen atoms have been omitted for clarity. In Fig. 2b and 2c, intermolecular Ag···Ag contacts are drawn with green dashed lines and H···F contacts are drawn with yellow dashed lines.

butyl groups. Additionally, the two benzene rings are outwards in the same disposition from the (carbene-C)$_4$ plane (δAg1(C$_4$) = 0.058, δAg2(C$_4$) = 0.046) with dihedral angles of 39.97° and 28.64°, respectively, which makes the cavity of **6b** look like a cone (Fig. 3a). The intramolecular Ag to Ag separation is 6.841 Å, which is similar to that of **6a**. The pairs of NHC rings in each bis-NHC ligand incline towards each other with dihedral angles of 40.99° and 49.82°, respectively, pointing to the same side of the (carbene-C)$_4$ plane. The pairs of NHC rings in each NHC–Ag–NHC unit are nearly coplanar, with dihedral angles of 5.52° and 4.84°, respectively.

As can be seen in Fig. 4a and 5a, due to the steric effects of the R^2 groups (naphylmethylene or anthrylmethylene) attached to the NHC rings, the cations of complexes **6c** and **6d** show rectangular configurations as a solid, which are very different from those of **6a** and **6b**. Complexes **6c** and **6d** crystallize in the $P\bar{1}$ and $C2/c$ space group, respectively. The cations of complexes **6c** and **6d** are both centrosymmetric. The intramolecular Ag to Ag separations in **6c** and **6d** are 9.235 Å and 8.859 Å, respectively. Two benzene rings in **6c** and **6d** are both parallel, with face-to-face distances of 4.927 Å and 5.071 Å, respectively, and the dihedral angles between the benzene rings and the corresponding (carbene-C)$_4$ planes of **6c** (δAg(C$_4$) = 0.032) and **6d** (δAg(C$_4$) = 0.021) are 77.24° and 82.44°, respectively. The dihedral angles between the pair of NHC rings within a ligand or in an NHC–Ag–NHC unit in **6c** and **6d** are larger than those in complexes **6a** and **6b**, with dihedral angles of 74.02° and 86.72°, respectively (Table 2).

Complexes **6e** and **6f** both crystallize in the $P\bar{1}$ space group. As depicted in Fig. 6a and 7a, 28-membered and 36-membered metallamacrocycles, formed by two linear NHC–Ag(I)–NHC axes and two flexible calixarene fragment linkers, can be observed in the structures of complexes **6e** and **6f**, respectively. The intramolecular Ag to Ag distances of complexes **6e** and **6f** are 12.546 Å and 16.986 Å, respectively, which are much longer than those of **6a–d**. In complex **6f**, the cation metallamacrocycle is centrosymmetric, whereas a symmetric center cannot be found in the cation of **6e** and there is a short contact between the silver cation and one oxygen atom of the methoxy group with a Ag2···O2 separation of 2.967(3) Å (smaller than the sum of the van der Waals radius 3.24 Å) (Fig. 6a). Owing to the low symmetry of the dinuclear cation of complex **6e**, the two pairs of benzene rings in *anti*-dispositions in two ligands (benzene rings A–A′ and B–B′ in Fig. 1, **6e**) are not parallel but form dihedral angles of 8.225° and 14.197°, respectively. The dihedral angles of the planes of the four benzene rings to the (carbene-C)$_4$ plane (δAg1(C$_4$) = 0.096, δAg2(C$_4$) = 0.118) of complex **6e** are disparate, with values of 66.99°, 63.38°, 7.93° and 22.15°. Comparably, in the cation of **6f**, the three pairs of benzene rings in *anti*-conformations in two ligands (A–A′, B–B′ and C, C′ in Fig. 1, **6f**) are parallel, with face-to-face distances of 3.758 Å, 8.900 Å and 8.184 Å, respectively. The dihedral angles between the planes of the benzene rings and the (carbene-C)$_4$ plane (δAg(C$_4$) = 0.013) for (A, A′), (B, B′) and (C, C′) are 63.43°, 41.62° and 73.19°, respectively. In addition, the pairs of NHC rings in each ligand of complexes **6e** and **6f** all point to the same side of the corresponding (carbene-C)$_4$ plane and the pairs of NHC rings in each NHC–Ag–NHC unit of

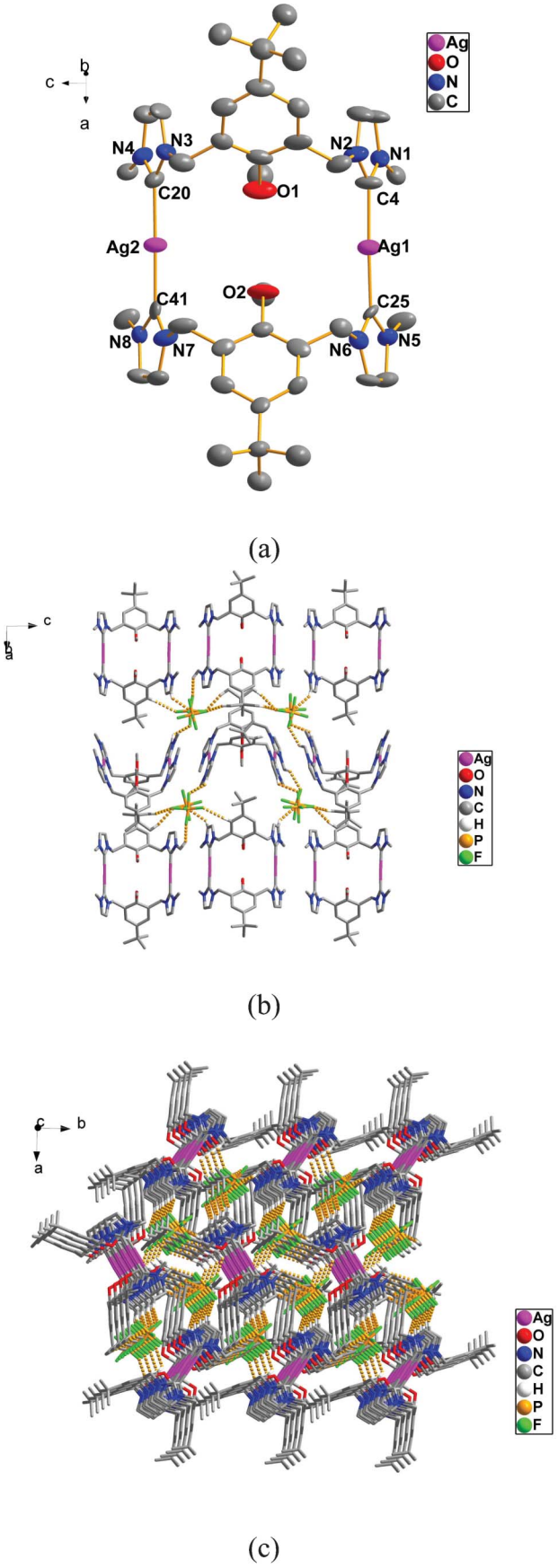

Fig. 3 (a) Molecular structure of complex **6b** (50% probability ellipsoids), hydrogen atoms and anions have been omitted for clarity. Selected bond lengths (Å) and angles (°): Ag1–C4 = 2.082(13) Å, Ag1–C25 = 2.085(12), Ag2–C41 = 2.084(14), Ag2–C20 = 2.102(14); C4–Ag1–C25 = 176.4(6), C41–Ag2–C20 = 177.3(6), N1–C4–N2 = 102.6(11), N4–C20–N3 = 104.7(12), N5–C25–N6 = 103.6(11), N7–C41–N8 = 103.9(11). (b) The 2D supramolecular layer of complex **6b** *via* intermolecular C–H···F hydrogen bonds. The irrelevant hydrogen atoms have been omitted for clarity. (c) The 3D supramolecular architecture of complex **6b** *via* intermolecular C–H···F hydrogen bonds. The irrelevant hydrogen atoms have been omitted for clarity. In (b and c), H···F contacts are drawn with yellow dashed lines.

complexes **6e** and **6f** are all arranged in opposite dispositions from the (carbene-C)$_4$ plane.

In particular, cation–π interactions between the silver cations and naphthalene rings or anthracene rings of R^2 adjacent to the same NHC unit are found in the structures of complex **6c–f** (Fig. 4a–7a). Although Ag(I)–arene interactions have been studied in many silver complexes,[23] reports of the interactions which exist in Ag(I)–NHC complexes are relatively limited.[24] As summarized in Table 3, the separations between the silver atoms and coordinating arene ring carbons of complexes **6a–f** are in the range of 2.993 Å to 3.4185 Å (smaller than the sum of the van der Waals radius, 3.42 Å).[25] The coordination modes between the silver atoms and arene π–electron systems generally follow η^2 or η^3-hapticity.[26] The distances of the silver atoms to the centers of the nearest six-membered interacting arene rings (d_1) are in the range of 3.252 Å to 3.860 Å and the relative perpendicular distances (d_2) are in the range of 2.802 Å to 3.114 Å. In complex **6c**, the silver atom coordinates with the C29 and C30 atoms of the naphthalene ring, with separations of 3.364(4) Å and 3.060(4) Å, indicating a η^2 coordination mode between the silver atom and the arene π–electron system. The distance of the silver atom to the centers of the nearest six-membered interacted arene ring is 3.776 Å, and the relative perpendicular distance is 2.8026 Å (Table 3). In contrast, the coordination mode of the silver cation with the anthracene π–electron system in complex **6d** follows a η^3-hapticity, coordinating with the C12, C13 and C14 atoms of the anthracene ring with separations of 3.229(7), 2.994(7) and 3.159(7) Å, respectively. The distance of the silver atoms to the centers of the nearest six-membered interacting arene rings is 3.410 Å and the relative perpendicular distance is 2.931 Å. In complexes **6e** and **6f**, the multi-arene linkers between two NHC–Ag(I)–NHC units in one molecule are more flexible. There are three groups of Ag(I)–arene π interactions between the two silver cations and three anthracene rings in **6e** and there are four groups in **6f** (Fig. 6a and 7a). The Ag(I)–arene π interactions exist more generally compared to those in **6c** and **6d**.

The crystal packing of complexes 6a–f

According to the analyses of the crystal packing of these complexes, it can be found that weak intermolecular interactions involve C–H···F hydrogen bonds (in **6a–f**), Ag···Ag interactions (in **6a**) and π–π interactions (in **6c–f**) and C–H···F hydrogen bonds[27] (Table S1, ESI†) play the most important role in the crystal packing of these complexes.

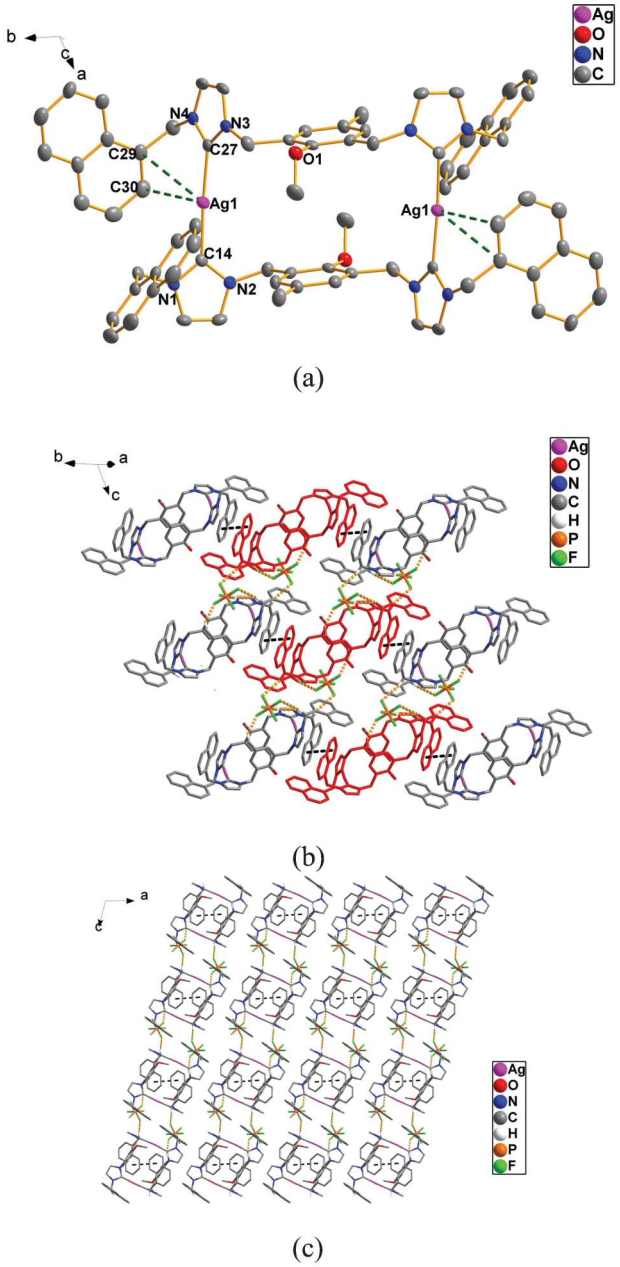

Fig. 4 (a) Molecular structure of complex **6c** (50% probability ellipsoids), hydrogen atoms and anions have been omitted for clarity. Selected bond lengths (Å) and angles (°): Ag1–C14 = 2.076(3), Ag1–C27A = 2.074(3); C14–Ag1–C27A = 175.25(10), N1–C14–N2 = 104.0(2), N3–C27–N4 = 104.1(2). (b) The 2D supramolecular layer of complex **6c** *via* intermolecular π–π interaction and C–H···F hydrogen bonds viewed along the *a* axis. The irrelevant hydrogen atoms have been omitted for clarity. (c) The 2D supramolecular layers of complex **6c** viewed along *b* axis. The irrelevant hydrogen atoms have been omitted for clarity. In (b and c), intermolecular π–π interactions are drawn with black dashed lines and H···F contacts are drawn with yellow dashed lines.

In the crystal packing of complex **6a**, weak intermolecular Ag···Ag interactions[28] are found with separations of 3.413 Å and a 3D architecture is assembled by these argentophilic contacts and intermolecular weak C–H···F interactions among the hydrogen atoms of the methyl groups attached to the NHC

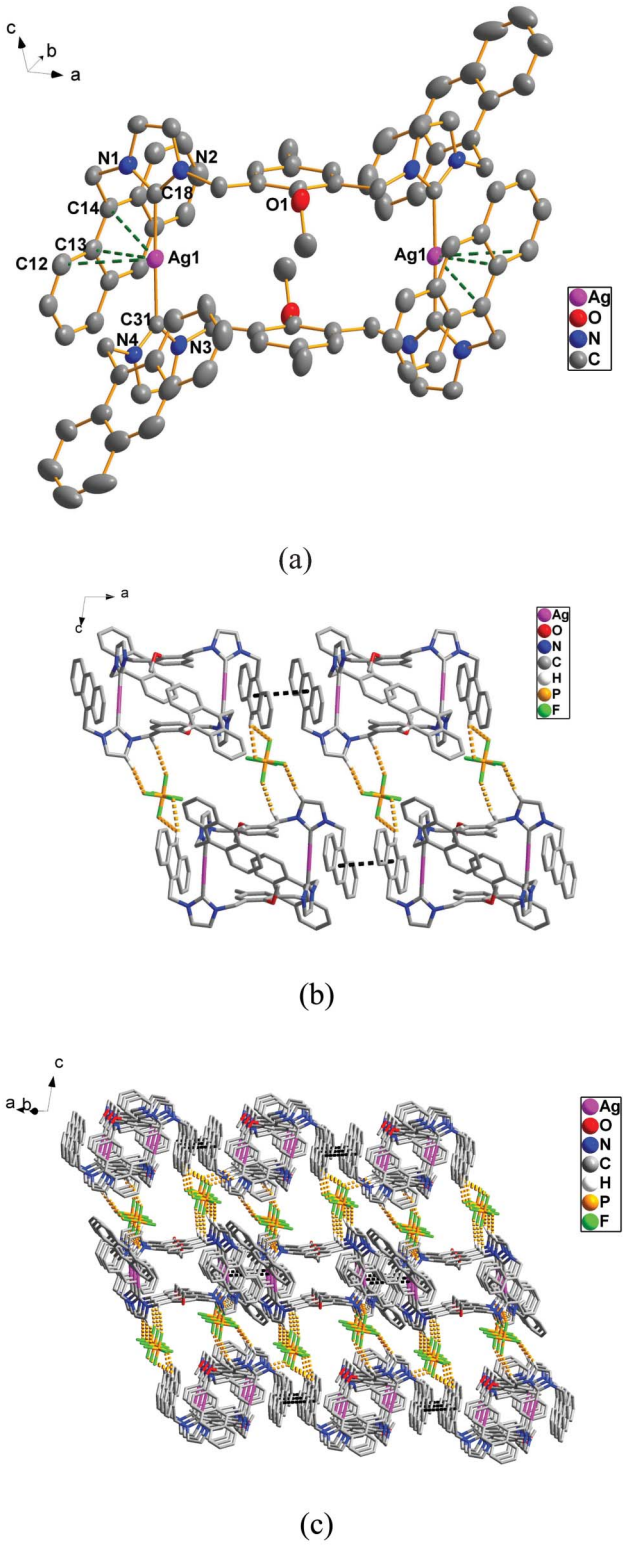

Fig. 5 (a) Molecular structure of complex **6d** (50% probability ellipsoids), hydrogen atoms and anions have been omitted for clarity. Selected bond lengths (Å) and angles (°): Ag1–C31 = 2.095(6), Ag1–C18A = 2.095(6), C18A–Ag1–C31 = 178.3(3), N2–C18–N1 = 105.2(5), N4–C31–N3 = 104.5(5). (b) The 2D supramolecular layer of complex **6d** *via* intermolecular π–π interaction and C–H···F hydrogen bonds viewed along the *b* axis. The irrelevant hydrogen atoms have been omitted for clarity. (c) The 3D supramolecular network of complex **6d**, viewed along the *a* axis. The irrelevant hydrogen atoms have been omitted for clarity. In (b and c), intermolecular π–π interactions are drawn with black dashed lines and H···F contacts are drawn with yellow dashed lines.

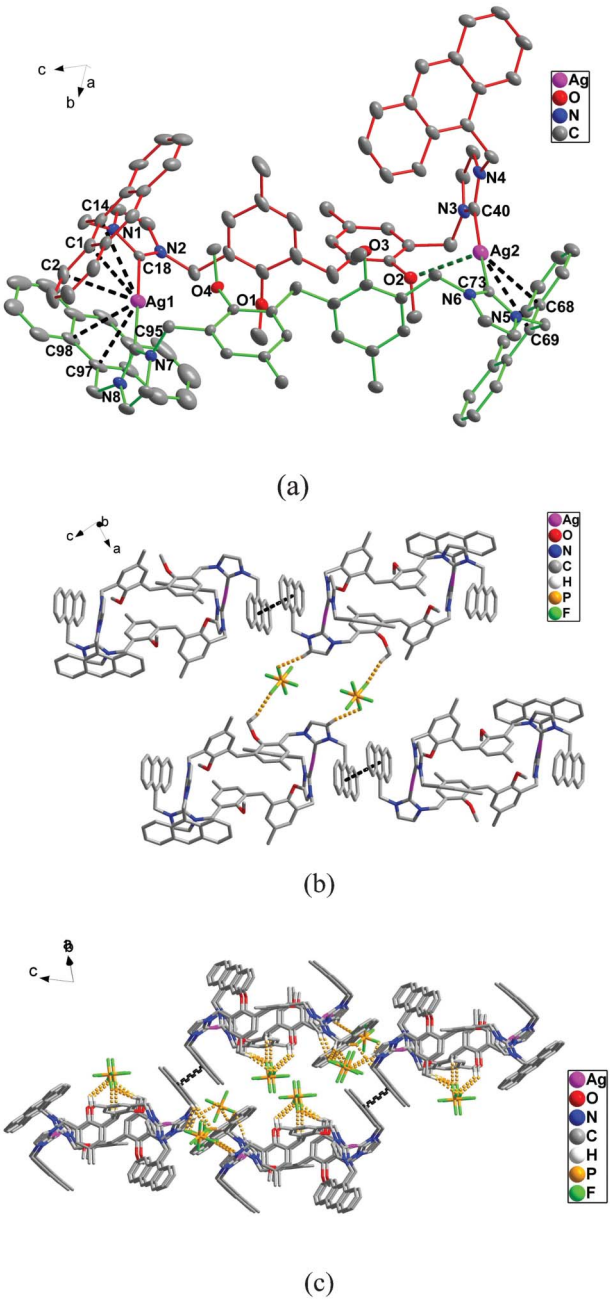

Fig. 6 (a) Molecular structure of complex **6e** (30% probability ellipsoids), hydrogen atoms and anions have been omitted for clarity. Selected bond lengths (Å) and angles (°): Ag1–C95 = 2.087(4), Ag1–C18 = 2.093(4), Ag2–C73 = 2.106(4), Ag2–C40 = 2.117(4), C95–Ag1–C18 = 174.17(2), C73–Ag2–C40 = 173.5(2), N2–C18–N1 = 104.1(3), N4–C40–N3 = 104.4(3), N5–C73–N6 = 103.8(3), N7–C95–N8 = 103.3(3). (b) The 2D supramolecular layer of complex **6e** *via* intermolecular π–π interaction and C–H···F hydrogen bonds viewed along the *b* axis. The irrelevant hydrogen atoms have been omitted for clarity. (c) The 3D supramolecular network of complex **6e** *via* intermolecular π–π interactions and C–H···F hydrogen bonds. The irrelevant hydrogen atoms have been omitted for clarity. In (b and c), intermolecular π–π interactions are drawn with black dashed lines and H···F contacts are drawn with yellow dashed lines.

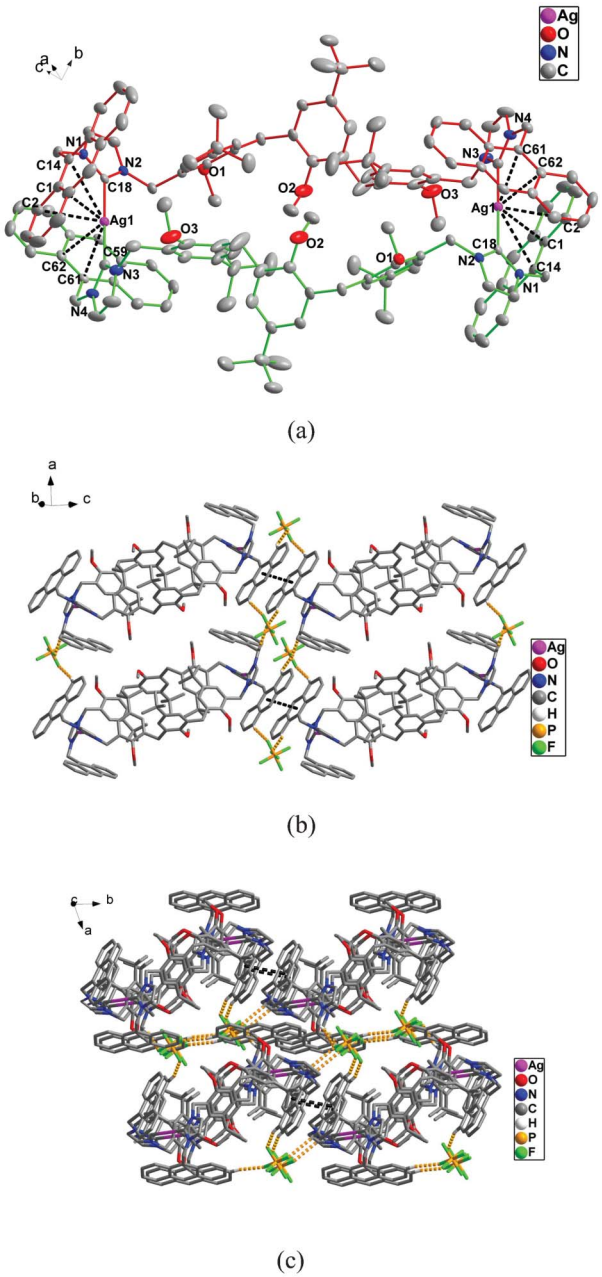

Fig. 7 (a) Molecular structure of complex **6f** (30% probability ellipsoids), hydrogen atoms have been omitted for clarity. Selected bond lengths (Å) and angles (°): Ag1–C18 = 2.093(3), Ag1–C59 = 2.090(3); C18–Ag1–C59A = 179.22(10), N2–C18–N1 = 104.3(2), N3–C59–N4 = 103.7(2). (b) The 2D supramolecular layer of complex **6f** *via* intermolecular π–π interaction and C–H···F hydrogen bonds. The irrelevant hydrogen atoms have been omitted for clarity. (c) The 3D supramolecular network of complex **6f** *via* intermolecular π–π interactions and C–H···F hydrogen bonds. The irrelevant hydrogen atoms have been omitted for clarity. In (b and c), intermolecular π–π interactions are drawn with black dashed lines and H···F contacts are drawn with yellow dashed lines.

rings and the fluorine atoms of hexafluorophosphate (C(1)–H(1B)···F(4) = 3.315(3) Å (0.5 + *x*, −0.5 + *y*, 0.5 − *z*) and C(1)–H(1C)···F(2) = 3.237(3) Å (1 − *x*, −*y*, *z*)) (Fig. 2b and 2c). However, in the lattice of complex **6b**, due to the steric hindrance of the *tert*-butyl groups, there is no intermolecular Ag···Ag interaction and the 3D network of **6b** is assembled directly by intermolecular C–H···F interactions in three dimensions (Fig. 3b and 3c).

Table 3 Structural features of **6d–f** with Ag(I)–arene π interactions

	d_1[a]/Å	d_2[b]/Å	Type[c]	d_3[d]/Å
6c	3.776	2.802	η^2	Ag1–C29 = 3.364(4), Ag1–C30 = 3.060(4)
6d	3.410	2.931	η^3	Ag1–C12 = 3.229(7), Ag1–C13 = 2.994(7), Ag1–C14 = 3.159(7)
6e[e]	3.853	3.098	η^3	Ag1–C1 = 3.308(5), Ag1–C2 = 3.354(5), Ag1–C14 = 3.382(5)
	3.253	3.085	η^2	Ag1–C97 = 3.110(5), Ag1–C98 = 3.262(7)
	3.860	3.114	η^3	Ag2–C67 = 3.418(5), Ag2–C68 = 3.347(4), Ag2–C69 = 3.370(4)
6f[f]	3.691	2.987	η^3	Ag1–C1 = 3.201(3), Ag1–C2 = 3.234(4), Ag1–C14 = 3.325(3)
	3.251	3.011	η^2	Ag1–C61 = 3.056(3), Ag1–C62 = 3.159(3)

[a] d_1 are the distances of the silver atoms to the centers of the nearest six-membered interacting arene rings. [b] d_2 are the perpendicular distances of the silver atoms to the nearest six-membered interacting arene rings. [c] The coordination modes between the silver atoms and arene π–electron systems. [d] d_3 are the distances of the silver atoms to the weak interacting C atoms of the arene interaction. [e] Three groups of intermolecular cation–π interactions between two Ag and three anthracenyl groups. [f] Four groups of cation–π interactions in two pairs between two Ag and four anthracenyl groups.

In complexes **6c–f**, π–π stackings[29] (Table S2, ESI†) between the intermolecular arene rings attached to the NHC rings are involved in the weak interactions. In complex **6c**, as can be seen in Fig. 4b and 4c, 2D supramolecular layers are formed *via* intermolecular C–H···F interactions and π–π stackings among the intermolecular naphthalene rings, with a face-to-face separation of 3.2915(13) Å (center-to-center separation of 3.820(2) Å). However, in complex **6d** a 3D network was assembled by the π–π contacts of the intermolecular anthracene rings, with a face-to-face separation of 3.367(3) Å (center-to-center separation = 3.955(4) Å) and C–H···F interactions (Fig. 5b and 5c). In the crystal packing of complexes **6e** and **6f**, similar π–π stacking interactions among the intermolecular anthracene rings are found, with a face-to-face distance of 3.4124(16) Å (center-to-center separation of 3.953(3) Å) for **6e** (Fig. 6b and 6c) and a face-to-face distance of 3.3705(11) Å (center-to-center separation of 3.6135(18) Å) for **6f** (Fig. 7b and 7c), respectively. 3D architectures of complexes **6e** and **6f** were formed *via* these π–π stacking interactions together with the intermolecular C–H···F interactions.

Fluorescent chemosensing behaviors

Fluorescent sensing behavior of complex 6d for *p*-benzoquinone. As mentioned above, since complex **6d** possesses a rectangular cavity, with an intramolecular Ag to Ag distance of 8.859 Å and two parallel benzene rings with a separation of 5.072 Å, it can enclose some small organic functional molecules. *p*-Benzoquinone (BQ) is a planar molecule with an O···O distance of 5.292 Å[30] and a complementary relationship of size and shape between **6d** and BQ is present. A fluorescence titration experiment of complex **6d** by BQ was carried out in acetonitrile at room temperature. As can be seen in Fig. 8a, after the gradual addition of BQ, the fluorescent emission intensity of **6d** sequentially decreased. When the BQ/**6d** molar ratio reached 5, the fluorescence of **6d** was completely quenched. The quenching was found to follow a conventional Stern–Volmer relationship[9b] and the association constant is estimated to be 2.45 × 10^4 M^{-1} (Fig. S18, ESI†). The Job plot analysis[31](Fig. 8b) indicates the formation of a 1 : 1 inclusion complex between **6d** and BQ (Scheme 2). However, when complexes **6e** and **6f** with larger cavities were

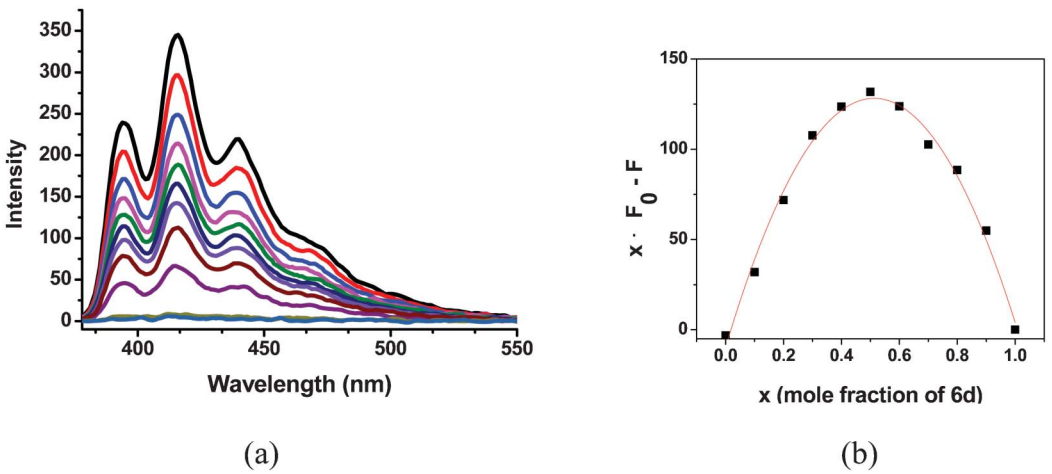

Fig. 8 (a) Fluorescence titration experiments of **6d** (1.0 × 10^{-5} mol L^{-1}) with increasing BQ concentration in acetonitrile (λ_{ex} = 370 nm) at room temperature. The concentrations of BQ for the curves from top to bottom are 0.0, 0.3, 0.4, 0.5, 0.6, 0.7, 0.8, 1.5, 2.5, 5.0, 8.0 × 10^{-5} mol L^{-1}. K_a = 2.45 × 10^4 M^{-1}. (b) Job plot of the fluorescence titration curves at 416 nm.

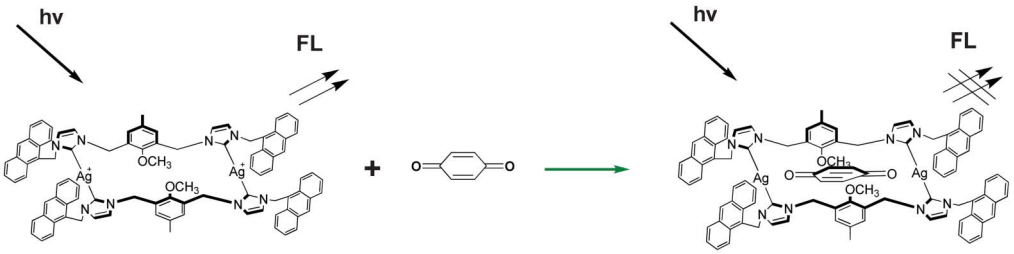

Scheme 2 Fluorescence titration of complex **6d** with *p*-benzoquinone (BQ).

applied as host molecules, no obvious quenching behaviors were observed at the same molar ratio of BQ/host, which indicates that complexes **6e** and **6f** cannot form the close 1 : 1 host–guest inclusion complexes with BQ. The fluorescent quenching may be attributed to a photo-induced electron transfer (PET) process between the functional NHC metallamacrocycle and BQ. Attempts to determine the solid-state structures of the inclusion complex were carried out but suitable single crystals for X-ray single crystal diffraction analysis were not obtained.

Sensing behaviors of complexes 6e and 6f for fullerenes. On the basis of our previous work in the recognition of C_{60} with $[(\mathbf{BIMAn})_2Ag_2](PF_6)_2$ (K_a = 3.48 × 10^5 M^{-1}),[15] the corresponding inclusion complexations when applying **6e** and **6f** as host molecules were studied through fluorescence titrations. Similar inclusion behaviors for C_{60} and C_{70} were observed and the fluorescence quenching behaviors were all found to follow a Stern–Volmer equation (Fig. S20–S23, ESI†). For complex **6e**, the association constants to C_{60} and C_{70} were 6.97 × 10^4 M^{-1} and 1.06 × 10^5 M^{-1}, respectively, and for complex **6f**, the association constants to C_{60} and C_{70} were 9.17 × 10^4 M^{-1} and 1.64 × 10^5 M^{-1}, respectively. As mentioned above, the association constant of $[(\mathbf{BIMAn})_2Ag_2](PF_6)_2$ for C_{60} is larger than that of complex **6e**, which suggests that receptors substituted with *tert*-butyl groups as the upper-rim may be more helpful for this kind of inclusive process. The association constants of the host molecule to C_{60} and C_{70} showed not much difference on comparing the approximate molecular sizes of C_{60} and C_{70} (with diameter of 7.1 and 8.0 Å, respectively). However, when complex **6d** was applied as a host molecule, the florescence intensity remained almost constant with the addition of fullerene. From these results, it can be induced that the size effect may play an important role in the sensing behavior for fullerenes. The quenching behaviors of **6e** and **6f** to C_{60} or C_{70} can be also attributed to a photo-induced electron transfer process between the metallamacrocycle system and the fullerenes.

Conclusions

A series of macrocyclic dinuclear bis-NHC Ag(I) complexes, **6a–f**, consisting of two NHC–Ag(I)–NHC units bridged with two calixarene fragments, have been designed and synthesized. The configurations of these complexes can be easily modified with the change of the upper-rims (R^1) of the calixarene fragments or the *N*-substituents (R^2) of the NHC rings. Cation–π interactions are formed between the silver cations and arene rings in complexes **6c–f**. In the crystal packing of the complexes, 2D supramolecular layers of **6c** and 3D supramolecular architectures of **6a**, **6b** and **6d–f** are formed *via* intermolecular C–H···F hydrogen bonds, intermolecular Ag···Ag interactions and π–π stackings. Additionally, complex **6d** showed excellent fluorescent chemosensing behavior for *p*-benzoquinone and complexes **6e** and **6f** exhibited recognition properties for C_{60} and C_{70} fullerenes. It can be anticipated that these kinds of metallamacrocycles can be further designed and synthesized and will exhibit more particular recognition behavior.

Experimental section

General procedure

All the reactions were carried out under a dry nitrogen atmosphere using standard Schlenk techniques unless stated otherwise. The solvents were purified by standard methods. The ESI-MS spectra were obtained on a Finnigan LCQ spectrometer. ^1H, ^{13}C and DOSY-NMR spectra were recorded on a Bruker AV400 spectrometer. Chemical shifts, δ, are reported in ppm relative to the internal standard TMS. *J* values are given in Hz. Elemental analyses were measured using a YanacoMT-3 elemental analyzer. The fluorescence spectra were measured with a Cary Eclipse fluorescence spectrophotometer. Compounds **3a–d** were prepared according to the literature.[16] Thermogravimetric analysis (TGA) and differential scanning calorimetry (DSC) analyses were performed using a NETZSCH STA 409 PC/PG instrument at a heating rate of 10 °C min^{-1} under high purity N_2 with a flow rate of 40 mL min^{-1}.

General procedure for the synthesis of precursors 5a–f

A 1,4-dioxane (30 mL) solution of bromide **3** (1.0 eq.) and *N*-substituted imidazole **4** (2.2 eq.) was refluxed for 2 days to give bisimidazolium bromide as a white solid. The bromide was dissolved in methanol (35 mL), NH_4PF_6 (1.96 g, 12 mmol) was added and the mixture was stirred for 3 h to precipitate a white solid. The solid was collected, washed with Et_2O and dried in a vacuum to give precursors **5a–f**.

[1-Methyl-3,5-bis(*N*-methylimidazol-2-yl)methyl-4-methoxybenzene] hexafluorophosphate 5a: 80%. ^1H NMR (400 MHz, DMSO-d_6): δ 9.12 (s, 2H, Im–H) (Im = imidazole), 7.70 (s, 4H,

Im–H), 7.16 (s, 2H, Ph–H) (Ph = benzene), 5.41 (s, 4H, Im–CH_2–Ph), 3.86 (s, 6H, Im–CH_3), 3.76 (s, 3H, –OCH_3), 2.26 (s, 3H, Im–CH_3); ^{13}C NMR (100 MHz, DMSO-d_6): δ 154.04 (C–OCH_3 of Ph), 136.81 (NCHN of Im), 134.63 (C–CH_3 of Ph), 131.37, 128.13, 123.84, 122.53 (Im), 62.09 (OCH_3), 47.26 (Im–CH_2–Ph), 35.81 (Im–CH_3), 20.23 (CH_3–Ph). ESI-MS $[M - PF_6^-]^+$: at *m*/*z* 457.2. Anal. calcd for $C_{18}H_{24}F_{12}N_4OP_2$: C, 47.27; H, 5.29; N, 12.25. Found: C, 47.24; H, 5.18; N, 12.45.

[1-(*Tert*-butyl)-3,5-bis(*N*-methylimidazol-2-yl)methyl-4-methoxybenzene] hexafluorophosphate 5b: 79%. ^{1}H NMR (400 MHz, DMSO-d_6): δ 9.11 (s, 2H, Im–H), 7.70 (s, 4H, Im–H), 7.47 (s, 2H, Ph–H), 5.42 (s, 4H, Im–CH_2–Ph), 3.86 (s, 6H, Im–CH_3), 3.76 (s, 3H, Ph–OCH_3), 1.26 (s, 9H, *t*-Bu); ^{13}C NMR (100 MHz, DMSO-d_6): δ 154.43 (C–OCH_3 of Ph), 147.91 (C–*t*-Bu of Ph), 136.66 (NCHN of Im), 128.74, 127.68, 123.80, 122.44 (Im), 62.08 (OCH_3), 47.71 (Im–CH_2–Ph), 35.82 (Im–CH_3), 34.31 (*t*-Bu), 30.93 (CH_3 of *t*-Bu). ESI-MS: $[M - PF_6^-]^+$: at *m*/*z* 499.2. Anal. calcd for $C_{21}H_{30}F_{12}N_4OP_2$: C, 39.14; H, 4.69; N, 8.69. Found: C, 39.04; H, 4.88; N 8.69.

[1-Methyl-3,5-bis(*N*-naphthylmethylimidazol-2-yl)methyl-4-methoxybenzene] hexafluorophosphate 5c: 89%. ^{1}H NMR (400 MHz, DMSO-d_6): δ 9.32 (s, 2H, Im–H), 8.10 (m, 2H, Naph–H) (Naph = Naphthalene), 8.04 (d, 4H, *J* = 8.0 Hz, Naph–H), 7.82 (s, 2H, Im–H), 7.69 (s, 2H, Im–H), 7.63–7.51 (m, 8H, Im–H and Naph–H), 7.01 (s, 2H, Ph–H), 5.94 (s, 4H, Naph–CH_2–Im), 5.40 (s, 4H, Im–CH_2–Ph), 3.60 (s, 3H, –OCH_3), 2.19 (s, 3H, –CH_3); ^{13}C NMR (100 MHz, DMSO-d_6): δ 153.92 (C–OCH_3 of Ph), 136.76 (NCHN of Im), 134.55 (C–CH_3 of Ph), 133.44, 131.01, 130.33, 129.89, 129.74, 127.17, 126.45, 125.64, 123.08, 122.93, 122.72, 61.81 (OCH_3), 50.08 (Im–CH_2–Naph), 47.52 (Im–CH_2–Ph), 20.25 (CH_3–Ph). ESI-MS $[M - PF_6^-]^+$: at *m*/*z* 709.3. Anal. calcd for $C_{38}H_{36}F_{12}N_4OP_2$: C, 53.40; H, 4.25; N, 6.56. Found: C, 53.19; H, 4.29; N, 5.75.

[1-Methyl-3,5-bis(*N*-anthrylmethylimidazol-2-yl)methyl-4-methoxybenzene] hexafluorophosphate 5d: 75%. ^{1}H NMR (400 MHz, DMSO-d_6): δ 9.04 (s, 2H, Im–H), 8.86 (s, 4H, An–H), (An = anthracene), 8.45 (d, 4H, *J* = 11.2 Hz, An–H), 8.23 (d, 4H, *J* = 10.8 Hz, An–H), 7.70–7.59 (m, 12H, Im–H and An–H), 6.83 (s, 2H, Ph–H), 6.51 (s, 4H, An–CH_2–Im), 5.28 (s, 4H, Im–CH_2–Ph), 3.40 (s, 3H, –OCH_3), 2.12 (s, 3H, –CH_3); ^{13}C NMR (100 MHz, DMSO-d_6): δ 153.54 (C–OCH_3 of Ph), 136.12 (NCHN of Im), 134.36 (C–CH_3 of Ph), 131.06, 130.57, 130.33, 130.16, 129.42, 128.27, 122.75, 126.59, 123.43, 123.26, 122.91, 122.77, 125.59, 123.43, 123.26, 122.91, 122.77, 61.51 (OCH_3), 47.25 (Im–CH_2–An), 45.02 (Im–CH_2–Ph), 20.27 (CH_3–Ph). ESI-MS $[M - PF_6^-]^+$: at *m*/*z* 809.3. Anal. calcd for $C_{46}H_{40}F_{12}N_4OP_2$: C, 57.87; H, 4.22; N, 5.87. Found: C, 57.84; H, 4.12; N, 5.57.

{Bis[3-(*N*-9-anthrylmethylimidazol-2-yl)methyl-5-methyl-2-methoxyphenyl]methane} hexafluorophosphate 5e: 73%. ^{1}H NMR (400 MHz, DMSO-d_6): δ 9.09 (s, 2H, NCHN), 8.86 (s, 2H, An–H), 8.47 (d, 4H, *J* = 8.7 Hz, An–H), 8.23 (d, 4H, *J* = 8.7 Hz, An–H), 7.69–7.60 (ddd, 12H, *J* = 14.7, 12.4, 7.1 Hz, An–H, Im–H), 6.74 (d, 4H, *J* = 9.0 Hz, Ph–H), 6.53 (s, 4H, An–CH_2), 5.30 (s, 4H, Im–CH_2), 3.84 (s, 2H, Ph–CH_2–Ph), 3.44 (s, 6H, 2-OCH_3), 2.09 (s, 6H, Ph–CH_3). ^{13}C NMR (100 MHz, DMSO-d_6): δ 153.83 (C–OCH_3 of Ph), 136.15 (NCHN of Im), 133.50, 133.41, 131.77, 131.08, 130.59, 130.15, 129.42, 128.04, 127.73, 127.67, 125.58, 123.52, 123.29, 122.82, 122.80, 60.94 (OCH_3), 47.86 (Im–CH_2–An), 44.99 (Im–CH_2–Ph), 28.33 (Ph–CH_2–Ph), 20.38 (CH_3–Ph). ESI-MS $[M - PF_6^-]^+$ at *m*/*z* 943.4. Anal. calcd for $C_{55}H_{50}F_{12}N_4O_2P_2$: C, 60.66; H, 4.63; N, 5.15. Found: C, 60.39; H, 4.63; N, 5.07.

5f: 68%. ^{1}H NMR (400 MHz, DMSO-d_6): δ 9.09 (s, 2H, NCHN), 8.86 (s, 2H, An–H), 8.48 (d, 4H, *J* = 8.8 Hz, An–H), 8.23 (d, 4H, *J* = 8.8 Hz, An–H), 7.69–7.60 (ddd, 12H, *J* = 17.5, 14.8, 6.2 Hz, An–H, Im–H), 7.02 (d, 2H, *J* = 2.1 Hz, Ph–H), 6.95 (d, 2H, *J* = 2.1 Hz, Ph–H), 6.92 (s, 2H, Ph–H), 6.55 (s, 4H, An–CH_2), 5.35 (s, 4H, Im–CH_2–Ph), 3.96 (s, 4H, Ph–CH_2–Ph), 3.51 (s, 6H, Ph–OCH_3 with Im), 3.44 (s, 3H, middle Ph–OCH_3), 1.07 (d, 27H, *J* = 16.1 Hz, *t*-Bu). ^{13}C NMR (100 MHz, DMSO-d_6): δ 152.91 (C–OCH_3 of Ph), 152.70 (C–OCH_3 of Ph), 145.35 (C–*t*-Bu of Ph), 144.60 (C–*t*-Bu of Ph), 134.84 (NCHN of Im), 132.43, 130.94, 129.99, 129.49, 129.05, 128.30, 127.21, 126.66, 125.99, 124.81, 124.46, 123.19, 122.39, 122.13, 121.71, 121.67, 59.71 (OCH_3), 59.21 (OCH_3), 47.08 (Im–CH_2–An), 43.85 (Im–CH_2–Ph), 32.80 (*t*-Bu), 32.71 (*t*-Bu), 29.88 (CH_3 of *t*-Bu), 29.75 (CH_3 of *t*-Bu), 27.95 (Ph–CH_2–Ph). ESI-MS $[M - PF_6^-]^+$ at *m*/*z* 1203.3. Anal. calcd for $C_{73}H_{78}F_{12}N_4O_3P_2$: C, 64.98; H, 5.83; N, 4.15. Found: C, 64.85; H, 5.69; N, 4.24.

General procedure for the synthesis of complexes 6a–f

A sample of precursor **5** (0.50 mmol) was dissolved in 50 mL of acetonitrile and silver oxide (1.0 mmol) was added to the solution. The mixture was stirred at 50 °C for 8 h with the exclusion of light. After cooling to room temperature, the suspension was filtered through Celite to collect the filtrate. The volatiles were evaporated *in vacuo* at room temperature. Pure complex **6** was afforded by recrystallization from acetonitrile–ethyl ether.

6a: 82%. ^{1}H NMR (400 MHz, DMSO-d_6): δ 7.47 (s, 8H, Im–H), 6.77 (s, 4H, Ph–H), 5.21 (s, 8H, Ph–CH_2–Ph), 3.82 (s, 12H, Im–CH_3), 3.56 (s, 6H, Ph–OCH_3), 2.04 (s, 6H, Ph–CH_3); ^{13}C NMR (100 MHz, DMSO-d_6): δ 179.35 (carbene), 152.04 (C–OCH_3 of Ph), 132.80, 129.22, 128.23, 121.99, 121.43, 117.03 (Im), 60.42 (OCH_3), 47.85 (Im–CH_2–Ph), 37.16 (Im–CH_3), 19.18 (CH_3–Ph); ESI-MS: $[M - 2PF_6^-]^{2+}/2$: at *m*/*z* 417.3 (for ^{107}Ag), 419.2 (for ^{109}Ag). Anal. calcd for $C_{36}H_{44}Ag_2F_{12}N_8O_2P_2$: C, 38.38; H, 3.94; N, 9.95. Found: C, 38.13; H, 4.19; N, 9.59.

6b: 85%. ^{1}H NMR (400 MHz, DMSO): δ 7.49 (s, 4H, Im–H), 7.08 (s, 4H, Ph–H), 5.23 (s, 8H, –CH_2–), 3.78 (s, 12H, Im–CH_3), 3.52 (s, 6H, Ph–OCH_3), 1.09 (s, 18H, *t*-Bu); ^{13}C NMR (100 MHz, DMSO-d_6): δ 179.40 (carbene), 152.22 (C–OCH_3 of Ph), 146.95 (C–*t*-Bu of Ph), 128.68, 125.07, 121.94, 121.34, 117.97 (Im), 60.41 (OCH_3), 48.07 (Im–CH_2–Ph), 37.14 (Im–CH_3), 32.94 (*t*-Bu), 29.73 (CH_3 of *t*-Bu); ESI-MS: at *m*/*z* $[M - 2PF_6^-]^{2+}/2$: at *m*/*z* 459.3 (for ^{107}Ag), 461.2 (for ^{109}Ag). Anal. calcd for $C_{42}H_{56}Ag_2F_{12}N_8O_2P_2$: C, 41.67; H, 4.66; N, 9.26, Found: C, 41.35; H, 4.96; N, 9.24.

6c: 70%. ^{1}H NMR (400 MHz, DMSO-d_6): δ 7.92 (t, 8H, *J* = 8.2 Hz, Naph–H), 7.83 (d, 4H, *J* = 8.0 Hz, Naph–H), 7.62 (d, 4H, *J* = 1.2 Hz, Im–H), 7.49 (t, 4H, *J* = 7.5 Hz, Naph–H), 7.40 (m, 8H, *J* = 1.2 Hz, *J* = 6.8 Hz, Im–H, Naph–H), 7.28 (t, 4H, *J* = 7.6 Hz, Naph–H), 7.22 (d, 4H, *J* = 6.8 Hz, Naph–H), 6.26 (s, 4H, Ph–H), 5.64 (s, 8H, Naph–CH_2–Im), 4.89 (s, 8H, Im–CH_2–Ph), 3.02 (s, 6H, –OCH_3), 1.75 (s, 6H, –CH_3); ^{13}C NMR (100 MHz, DMSO-d_6): δ 179.78 (carbene), 151.58 (C–OCH_3 of Ph), 132.51, 132.37,

131.34, 129.38, 128.94, 127.82, 127.67, 127.40, 125.91, 125.57, 125.10, 124.26, 122.04, 121.93, 121.17, 117.00 (Im), 59.92 (OCH_3), 51.03 (Im–CH_2–Naph), 48.23 (Im–CH_2–Ph), 19.13 (CH_3–Ph); ESI-MS $[M - 2PF_6^-]^{2+}/2$: at *m*/*z* 669.4 (for ^{107}Ag), 671.3 (for ^{109}Ag). Anal. calcd for $C_{76}H_{68}Ag_2F_{12}N_8O_2P_2$: C, 55.96; H, 4.20; N, 6.87. Found: C, 55.98; H, 4.39; N, 6.66.

6d: 73%. ^1H NMR (400 MHz, DMSO-d_6): δ 8.66 (s, 4H, An–H), 8.329 (d, 8H, J = 8.9 Hz, An–H), 8.05 (d, 8H, J = 8.4 HZ, An–H), 7.60 (d, 4H, J = 1.2 HZ, Im–H), 7.52 (m, 8H, An–H), 7.41 (m, 8H, An–H), 7.15 (d, 4H, J = 1.2 HZ, Im–H), 6.05 (s, 8H, An–CH_2–Im), 5.28 (s, 8H, Ph–H), 4.15 (s, 8H, Im–CH_2–Ph), 2.29 (s, 6H, –OCH_3), 1.08 (s, 6H, –CH_3); ^{13}C NMR (100 MHz, DMSO-d_6): δ 181.01 (carbene), 151.22 (C–OCH_3 of Ph), 132.65, 131.03, 130.07, 129.06, 128.85, 127.06, 126.81, 126.38, 125.20, 123.71, 123.22, 121.20, 60.02 (OCH_3), 48.82 (Im–CH_2–An), 45.99 (Im–CH_2–Ph), 19.70 (CH_3–Ph). ESI-MS $[M - 2PF_6^-]^{2+}/2$: at *m*/*z* 769.2 (for ^{107}Ag), 771.2 (for ^{109}Ag). Anal. calcd. for $C_{92}H_{76}Ag_2F_{12}N_8O_2P_2$: C, 60.34; H, 4.18; N, 6.12. Found: C, 60.40; H, 4.13; N, 6.16.

6e: 75%. ^1H NMR (400 MHz, DMSO-d_6) δ 8.70 (s, 4H, An–H), 8.22 (d, 8H, J = 8.7 Hz, An–H), 8.08 (d, 8H, J = 8.2 Hz, An–H), 7.75 (s, 4H, Im–H), 7.53–7.42 (m, 16H, An–H), 7.34 (s, 4H, Im–H), 6.07 (d, 10H, J = 27.1 Hz, Ph–H, An–CH_2–Im), 5.88 (s, 4H, Ph–H), 4.16 (s, 8H, Im–CH_2–Ph), 2.98 (s, 4H, Ph–CH_2–Ph), 2.50 (s, 12H, –OCH_3), 1.60 (s, 12H, Ph–CH_3). ^{13}C NMR (100 MHz, DMSO-d_6): δ 181.01 (carbene), 180.84 (carbene), 179.02 (carbene), 178.90 (carbene), 152.86 (C–OCH_3 of Ph), 132.68, 132.57, 131.04, 130.15, 129.14, 129.07, 128.87, 126.93, 126.68, 125.18, 123.79, 123.24, 121.04 (Im), 59.94 (OCH_3), 50.01 (Im–CH_2–An), 46.01 (Im–CH_2–Ph), 26.61 (Ph–CH_2–Ph), 20.04 (CH_3–Ph). ESI-MS $[M - 2PF_6^-]^{2+}/2$: at *m*/*z* 903.5 (for ^{107}Ag), 905.5 (for ^{109}Ag). Anal. calcd. for $C_{110}H_{96}F_{12}N_8O_4P_2$: C, 62.92; H, 4.61; N, 5.34. Found: C 62.65; H, 4.32; N, 5.61.

6f: 73%. ^1H NMR (400 MHz, DMSO-d_6): δ 8.73 (s, 4H, An–H), 8.34 (d, 8H, J = 8.9 Hz, An–H), 8.07 (d, 8H, J = 8.4 Hz, An–H), 7.88 (s, 4H, Im–H), 7.60–7.58 (m, 8H, An–H), 7.40–7.36 (m, 8H, An–H), 7.32 (s, s, 4H, Im–H), 6.59 (s, 4H, Ph–H), 6.48 (s, 4H, Ph–H), 6.11 (s, 8H, An–CH_2–Im), 5.87 (s, 4H, Ph–H), 4.11 (s, 8H, Im–CH_2–Ph), 3.54 (s, 8H, Ph–CH_2–Ph), 3.14 (s, 6H, 2-OCH_3 of middle Ph), 2.54 (s, 12H, 4-OCH_3), 0.98 (s, 18H, *t*-Bu of middle Ph), 0.43 (s, 36H, *t*-Bu). ^{13}C NMR (100 MHz, DMSO-d_6): δ 180.54 (carbene), 180.40 (carbene), 178.57 (carbene), 178.43 (carbene), 154.57 (C–OCH_3 of Ph), 152.39 (C–OCH_3 of Ph), 145.49 (C–*t*-Bu of Ph), 145.36 (C–*t*-Bu of Ph), 132.80, 131.70, 131.08, 130.15, 129.10, 128.93, 128.28, 127.11, 127.05, 126.56, 125.73, 125.15, 123.80, 121.06 (Im), 60.31 (OCH_3), 60.05 (OCH_3), 49.69 (Im–CH_2–An), 45.87 (Im–CH_2–Ph), 33.70 (*t*-Bu), 33.19 (*t*-Bu), 30.97 (CH_3 of *t*-Bu), 30.28 (CH_3 of *t*-Bu), 28.37 (Ph–CH_2–Ph). ESI-MS $[M - 2PF_6^-]^{2+}/2$: at *m*/*z* 1163.5 (for ^{107}Ag), 1165.5 (for ^{109}Ag). Anal. calcd for $C_{146}H_{152}A_{g2}F_{12}N_8O_6P_2$: C, 66.92; H, 5.85; N, 4.28. Found: C, 66.78; H, 5.69; N, 4.07.

Crystallography

Single crystals of complexes **6a–f** suitable for X-ray diffraction analysis were obtained by the slow diffusion of diethyl ether into their acetonitrile–ethanol solutions at room temperature, respectively. Diffraction intensity data of **6a–f** were all collected at 113(2) K on a Rigaku Saturn724 CCD diffractometer using Mo–Kα radiation (0.71073 Å). Absorption corrections were performed using CrystalClear. All the structures were solved using direct methods, which yielded the positions of all non-hydrogen atoms. These were refined first isotropically and then anisotropically. For the structure of **6a**, each asymmetric unit contains 0.5 Et_2O solvent molecules. The diethyl ether molecule is disordered and the atoms (C12–C15, O3) are assigned to a partial site-occupancy of 0.25, respectively. For the structure of **6b**, the *tert*-butyl group and two PF_6 anions are disordered and the atoms (C14–C16, F1–F6 and F7–F12) are assigned to partial site-occupancies of 0.548, 0.803 and 0.559, respectively. The final R indices (0.1235 and 0.2169 for R_1 and wR_2, respectively) are a little high because of many uses of restrains (470 restraints for 760 parameters) to resolve the disordered groups in the molecule. The single crystal of **6b** has been grown in other mixed solvents but could not be obtained in better quality. For the structure of **6c**, each asymmetric unit contains 2 CH_3CN crystallized solvent molecules. The naphthylmethyl group and PF_6 anion are disordered and the atoms (C28–C38) and (F1–F4) are assigned to partial site-occupancies of 0.744 and 0.676, respectively. For the structure of **6d**, each asymmetric unit contains 4.5 CH_3CN, 0.5 Et_2O and 1.0 H_2O crystallized solvents. The atoms (C55, C56, N7), (C57, C58, N8), (C59, C60, N9), (C51–C54, O2), O3, O4 and O4′ are assigned to partial site-occupancies of 0.25, 0.3, 0.2 and 0.25, 0.25, 0.125 and 0.125, respectively. The hydrogens attached to the disordered solvents were not added. For the structure of **6e**, each asymmetric unit contains 1.5 CH_3CN solvent molecules. For the structure of **6f**, each asymmetric unit contains 2 CH_3CN solvent molecules. One of the CH_3CN molecules is disordered and the atoms (C75, C76 and N5) are assigned to a partial site-occupancy of 0.6. Furthermore, two methoxy groups and the PF_6 anion of **6f** are disordered and the atoms C42, C54 and F1–F6 are assigned to partial site-occupancies of 0.6, 0.5 and 0.852, respectively. All of the disordered parts were restrained using DFIX, ISOR and SIMU instructions to make the displacement parameters more reasonable. It should be noted that the ADPs for some atoms in **6e** are a bit large because these long chain atoms or groups in the macrocyclic frame are slightly disordered. Attempts to solve these atoms into two positions with suitable variable site-occupations were not satisfied. All the hydrogen atoms of the ligand were placed in calculated positions with fixed isotropic thermal parameters and were included in the structure factor calculations in the final stage of the full-matrix least-squares refinement.

All the calculations were performed using the SHELXTL system of computer programs.[32] The crystallographic data are summarized in Table 4 for **6a–c** and Table 5 for **6e–f**.

Acknowledgements

This work is supported by the National Natural Science Foundation of China (No. 21172114, No. 21172036).

Table 4 Summary of crystallographic data for complexes **6a–c**

	6a·Et_2O	**6b**	**6c**·$2CH_3CN$
CCDC	898036	906066	898037
Chemical formula	$C_{40}H_{54}Ag_2F_{12}N_8O_3P_2$	$C_{42}H_{56}Ag_2F_{12}N_8O_2P_2$	$C_{80}H_{74}Ag_2F_{12}N_{10}O_2P_2$
Formula weight	1200.57	1210.63	1713.17
Crystal system	Orthorhombic	Monoclinic	Triclinic
Space group	*Ibam*	*P*2(1)/*n*	$P\bar{1}$
a (Å)	12.616(4)	20.903(4)	11.967(3)
b (Å)	18.479(5)	10.785(3)	13.539(3)
c (Å)	20.409(6)	21.922(7)	13.776(4)
α (°)	90	90	116.722(12)
β (°)	90	90.808(13)	96.41(2)
γ (°)	90	90	103.815(17)
Volume (Å^3)	4758(2)	4942(2)	1873.2(8)
Z	8	4	1
D_{calcd} (g cm^{-3})	1.676	1.627	1.519
Abs coeff (mm^{-1})	0.984	0.947	0.650
F(000)	2424	2448	872
Crystal size (mm)	0.20 × 0.18 × 0.12	0.18 × 0.16 × 0.12	0.30 × 0.22 × 0.16
θ_{min}, θ_{max}/°	1.95, 25.03	1.34 to 24.99	2.09 to 25.03
Reflections collected/unique	21 462/2166	29 406/8468	16 051/6588
R_{int}	0.0321	0.0889	0.0501
Max. and min. transmission	0.8910, 0.8275	0.8948, 0.8480	0.9031, 0.8288
Data/restraints/parameters	42 166/72/193	8468/470/760	6588/540/624
Goodness-of-fit on F^{2a}	1.041	1.032	0.986
Final *R* indices^b [$I > 2s(I)$] R_1, wR_2	0.0276, 0.0780	0.1235, 0.2169	0.0345, 0.0688
R and R_w (all data) R_1, wR_2	0.0287, 0.0790	0.1667, 0.2438	0.0415, 0.0713
Largest diff. peak and hole (e Å^{-3})	0.836 and −0.405	1.141 and −0.916	0.507 and −0.666

^{a} Goof = $[\Sigma w(F_o^2 - F_c^2)^2/(n-p)]^{1/2}$, where *n* is the number of reflections and *p* is the number of parameters refined. ^{b} $R_1 = \Sigma(||F_o| - |F_c||)/\Sigma|F_o|$; $wR_2 = 1/[\sigma^2(F_o^2) + (0.0691P) + 1.4100P]$ where $P = (F_o^2 + 2F_c^2)/3$.

Table 5 Summary of crystallographic data for complexes **6d–f**

	6d·$4.5CH_3CN{\cdot}0.5Et_2O{\cdot}H_2O$	**6e**·$1.5CH_3CN$	**6f**·$4CH_3CN$
CCDC	898043	931824	930716
Formula	$C_{103}H_{96.5}Ag_2F_{12}N_{11}O_{4.50}P_2$	$C_{113}H_{101\cdot50}Ag_2F_{12}N_{9\cdot50}O_4P_2$	$C_{154}H_{164}Ag_2F_{12}N_{12}O_6P_2$
Formula weight	2066.1	2162.22	2784.66
Crystal system	Monoclinic	Triclinic	Triclinic
Space group	*C*2/*c*	$P\bar{1}$	$P\bar{1}$
a (Å)	16.080(6)	15.946(3)	12.733(2)
b (Å)	26.639(9)	17.488(3)	15.734(3)
c (Å)	25.248(8)	19.160(3)	19.262(4)
α (°)	90.00	68.336(4)	83.265(8)
β (°)	98.115(6)	85.729(9)	80.083(8)
γ (°)	90.00	86.013(9)	70.440(6)
Volume (Å^3)	10 706(6)	4946.8(16)	3574.7(11)
Z	4	2	1
D_{calcd} (g cm^{-3})	1.284	1.451	1.294
Abs coeff (mm^{-1})	0.469	0.511	0.371
F(000)	4238	2218	1452
Crystal size (mm)	0.20 × 0.20 × 0.10	0.20 × 0.18 × 0.12	0.20 × 0.18 × 0.12
θ_{min}, θ_{max}/°	1.49, 25.02	1.25 to 25.02	1.38 to 25.02
Reflections collected/unique	39 764/9393	41 166/17 387	30 722/12 570
R_{int}	0.0918	0.0366	0.0360
Max. and min. transmission	0.9546 and 0.9120	0.9412, 0.9047	0.9568, 0.9295
Data/restraints/parameters	9393/369/726	17 387/57/1340	12 570/485/997
Goodness-of-fit on F^{2a}	1.109	1.056	1.047
Final *R* indices^b [$I > 2s(I)$], R_1, wR_2	0.0906, 0.2328	0.0543, 0.1345	0.0414, 0.1159
R and R_w (all data), R_1, wR_2	0.1036, 0.2443	0.0656, 0.1423	0.0465, 0.1189
Largest diff. peak and hole (e Å^{-3})	0.943 and −0.713	1.315 and −0.781	0.966 and −0.529

^{a} Goof = $[\Sigma w(F_o^2 - F_c^2)^2/(n-p)]^{1/2}$, where *n* is the number of reflections and *p* is the number of parameters refined. ^{b} $R_1 = \Sigma(||F_o| - |F_c||)/\Sigma|F_o|$; $wR_2 = 1/[\sigma^2(F_o^2) + (0.0691P) + 1.4100P]$ where $P = (F_o^2 + 2F_c^2)/3$.

References

1 (*a*) C. Boehme and G. Frenking, *J. Am. Chem. Soc.*, 1996, **118**, 2039–2046; (*b*) M. S. Viciu, O. Navarro, R. F. Germaneau, R. A. Kelly, W. Sommer, N. Marion, E. D. Stevens, L. Cavallo and S. P. Nolan, *Organometallics*, 2004, **23**, 1629–1635; (*c*) O. Kühl, *Functionalised N-Heterocyclic Carbene Complexes*, John Wiley & Sons Ltd., Chichester, UK, 2010.

2 (*a*) P. de Frémont, N. Marion and S. P. Nolan, *Coord. Chem. Rev.*, 2009, **253**, 862–892; (*b*) W. A. Herrmann, *Angew. Chem., Int. Ed.*, 2002, **41**, 1290–1309.

3 (*a*) F. E. Hahn and M. C. Jahnke, *Angew. Chem., Int. Ed.*, 2008, **47**, 3122–3172; (*b*) H. D. Velazquez and F. Verpoort, *Chem. Soc. Rev.*, 2012, **41**, 7032–7060; (*c*) S. P. Nolan, *Acc. Chem. Res.*, 2010, **44**, 91–100; (*d*) R. Credendino, L. Falivene and L. Cavallo, *J. Am. Chem. Soc.*, 2012, **19**, 8127–8135.

4 (*a*) K. M. Hindi, M. J. Panzner, C. A. Tessier, C. L. Cannon and W. J. Youngs, *Chem. Rev.*, 2009, **109**, 3859–3884; (*b*) J. C. Y. Lin, R. T. W. Huang, C. S. Lee, A. Bhattacharyya, W. S. Hwang and I. J. B. Lin, *Chem. Rev.*, 2009, **109**, 3561–3598.

5 (*a*) M. C. Gimeno, A. Laguna and R. Visbal, *Organometallics*, 2012, **31**, 7146–7157; (*b*) C.-F. Chang, Y.-M. Cheng, Y. Chi, Y.-C. Chiu, C.-C. Lin, G.-H. Lee, P.-T. Chou, C.-C. Chen, C.-H. Chang and C.-C. Wu, *Angew. Chem., Int. Ed.*, 2008, **47**, 4542–4545.

6 L. Mercs and M. Albrecht, *Chem. Soc. Rev.*, 2010, **39**, 1903–1912.

7 (*a*) R. Maity, A. Rit, C. Schulte to Brinke, C. G. Daniliuc and F. E. Hahn, *Chem. Commun.*, 2013, **49**, 1011–1013; (*b*) A. Rit, T. Pape, A. Hepp and F. E. Hahn, *Organometallics*, 2011, **30**, 334–347.

8 (*a*) J. Gil-Rubio, V. Cámara, D. Bautista and J. Vicente, *Inorg. Chem.*, 2013, **7**, 4071–4083; (*b*) M. Baron, C. Tubaro, M. Basato, A. Biffis, M. M. Natile and C. Graiff, *Organometallics*, 2011, **30**, 4607–4615; (*c*) Q.-X. Liu, X.-Q. Yang, X.-J. Zhao, S.-S. Ge, S.-W. Liu, Y. Zang, H.-b. Song, J.-H. Guo and X.-G. Wang, *CrystEngComm*, 2010, **12**, 2245–2255; (*d*) C. A. Quezada, J. C. Garrison, M. J. Panzner, C. A. Tessier and W. J. Youngs, *Organometallics*, 2004, **23**, 4846–4848; (*e*) T. A. P. Paulose, S.-C. Wu, J. A. Olson, T. Chau, N. Theaker, M. Hassler, J. W. Quail and S. R. Foley, *Dalton Trans.*, 2012, **41**, 251–260; (*f*) F. Jean-Baptiste dit Dominique, H. Gornitzka and C. Hemmert, *J. Organomet. Chem.*, 2008, **693**, 579–583.

9 (*a*) A. Rit, T. Pape and F. E. Hahn, *Organometallics*, 2011, **30**, 6393–6401; (*b*) Q.-X. Liu, Z.-Q. Yao, X.-J. Zhao, A.-H. Chen, X.-Q. Yang, S.-W. Liu and X.-G. Wang, *Organometallics*, 2011, **30**, 3732–3739; (*c*) M. A. Iqbal, R. A. Haque, M. B. K. Ahamed, A. M. S. A. Majid and S. S. Al-Rawi, *Med. Chem. Res.*, 2012, **22**, 1–12; (*d*) Q. X. Liu, H. Wang, X. J. Zhao, Z. Q. Yao, Z. Q. Wang, A. H. Chen and X. G. Wang, *CrystEngComm*, 2012, **14**, 5330–5348; (*e*) M. A. Iqbal, R. A. Haque, S. Budagumpi, M. B. Khadeer Ahamed and A. M. S. Abdul Majid, *Inorg. Chem. Commun.*, 2013, **28**, 64–69; (*f*) D. C. F. Monteiro, R. M. Phillips, B. D. Crossley, J. Fielden and C. E. Willans, *Dalton Trans.*, 2012, **41**, 3720–3725; (*g*) U. J. Scheele, M. Georgiou, M. John, S. Dechert and F. Meyer, *Organometallics*, 2008, **27**, 5146–5151.

10 (*a*) X.-J. Wan, F.-B. Xu, Q.-S. Li, H.-B. Song and Z.-Z. Zhang, *Inorg. Chem. Commun.*, 2005, **8**, 1053–1055; (*b*) J.-W. Wang, L.-Y. Gao, F.-H. Meng, J. Jiao, L.-Y. Ding and L.-F. Zhang, *J. Inclusion Phenom. Macrocyclic Chem.*, 2012, **73**, 119–128.

11 (*a*) P. J. Barnard, L. E. Wedlock, M. V. Baker, S. J. Berners-Price, D. A. Joyce, B. W. Skelton and J. H. Steer, *Angew. Chem., Int. Ed.*, 2006, **45**, 5966–5970; (*b*) F. Jean-Baptiste dit Dominique, H. Gornitzka, A. Sournia-Saquet and C. Hemmert, *Dalton Trans.*, 2009, 340–352; (*c*) M. Baron, C. Tubaro, A. Biffis, M. Basato, C. Graiff, A. Poater, L. Cavallo, N. Armaroli and G. Accorsi, *Inorg. Chem.*, 2012, **51**, 1778–1784.

12 (*a*) R. A. Haque, M. A. Iqbal, S. Budagumpi, M. B. Khadeer Ahamed, A. M. S. Abdul Majid and N. Hasanudin, *Appl. Organomet. Chem.*, 2013, **27**, 214–223; (*b*) R. A. Haque, M. Z. Ghdhayeb, A. W. Salman, S. Budagumpi, M. B. Khadeer Ahamed and A. M. S. Abdul Majid, *Inorg. Chem. Commun.*, 2012, **22**, 113–119.

13 (*a*) M. Shah and Y. Agrawal, *J. Sci. Ind. Res.*, 2012, **71**, 21–26; (*b*) B. Mokhtari, K. Pourabdollah and N. Dallali, *J. Radioanal. Nucl. Chem.*, 2011, **287**, 921–934; (*c*) F. T. Minhas, S. Memon and M. Bhanger, *J. Inclusion Phenom. Macrocyclic Chem.*, 2010, **67**, 295–302.

14 (*a*) E. K. Bullough, M. A. Little and C. E. Willans, *Organometallics*, 2013, **32**, 570–577; (*b*) T. Fahlbusch, M. Frank, G. Maas and J. Schatz, *Organometallics*, 2009, **28**, 6183–6193; (*c*) M. Frank, G. Maas and J. Schatz, *Eur. J. Org. Chem.*, 2004, 607–613; (*d*) I. Dinarès, C. Garcia de Miguel, M. Font-Bardia, X. Solans and E. Alcalde, *Organometallics*, 2007, **26**, 5125–5128.

15 D.-B. Qin, X.-X. Zeng, Q.-X. Li, F.-B. Xu, H.-B. Song and Z.-Z. Zhang, *Chem. Commun.*, 2007, 147–149.

16 (*a*) B. Dhawan and C. Gutsche, *J. Org. Chem.*, 1983, **48**, 1536–1539; (*b*) B. Masci, M. Finelli and M. Varrone, *Chem.–Eur. J.*, 1998, **4**, 2018–2030; (*c*) T. Haino, K. Matsumura, T. Harano, K. Yamada, Y. Saijyo and Y. Fukazawa, *Tetrahedron*, 1998, **54**, 12185–12196.

17 J. C. Garrison and W. J. Youngs, *Chem. Rev.*, 2005, **105**, 3978–4008.

18 L. Benhamou, E. Chardon, G. Lavigne, S. Bellemin-Laponnaz and V. César, *Chem. Rev.*, 2011, **111**, 2705–2733.

19 Z. Lu, S. A. Cramer and D. M. Jenkins, *Chem. Sci.*, 2012, **3**, 3081–3087.

20 (*a*) R. S. Hickok, S. A. Wedge, A. L. Hansen, K. F. Morris, F. H. Billiot and I. M. Warner, *Magn. Reson. Chem.*, 2002, **40**, 755–761; (*b*) R. Takano, K. Furumoto, K. Shiraki, N. Takata, Y. Hayashi, Y. Aso and S. Yamashita, *Pharm. Res.*, 2008, **25**, 2334–2344.

21 (*a*) M. K. Samantaray, V. Katiyar, K. Pang, H. Nanavati and P. Ghosh, *J. Organomet. Chem.*, 2007, **692**, 1672–1682; (*b*) M. K. Samantaray, V. Katiyar, D. Roy, K. Pang, H. Nanavati, R. Stephen, R. B. Sunoj and P. Ghosh, *Eur. J. Inorg. Chem.*, 2006, **2006**, 2975–2984.

22 P. J. Barnard, M. V. Baker, S. J. Berners-Price, B. W. Skelton and A. H. White, *Dalton Trans.*, 2004, 1038–1047.

23 (*a*) Y. Hitomi, T. Nagai and M. Kodera, *Chem. Commun.*, 2012, **48**, 10392–10394; (*b*) P. Pérez-Gaán, N. Delpont, E. Herrero-Gómez, F. Maseras and A. M. Echavarren, *Chem.–Eur. J.*, 2010, **16**, 5324–5332; (*c*) P. Pérez-Galán, N. Delpont, E. Herrero-Gómez, F. Maseras and A. M. Echavarren, *Chem.–Eur. J.*, 2011, **17**, 12537.

24 X. Liu, R. Pattacini, P. Deglmann and P. Braunstein, *Organometallics*, 2011, **30**, 3302–3310.

25 A. Bondi, *J. Phys. Chem.*, 1964, **68**, 441–451.
26 (*a*) M. Munakata, L. P. Wu, T. Kuroda-Sowa, M. Maekawa, Y. Suenaga, G. L. Ning and T. Kojima, *J. Am. Chem. Soc.*, 1998, **120**, 8610–8618; (*b*) F.-B. Xu, L.-H. Weng, L.-J. Sun, Z.-Z. Zhang and Z.-F. Zhou, *Organometallics*, 2000, **19**, 2658–2660; (*c*) Z. Ma, F. E. Jacobsen and D. P. Giedroc, *Chem. Rev.*, 2009, **109**, 4644–4681.
27 J. C. Mareque Rivas and L. Brammer, *Coord. Chem. Rev.*, 1999, **183**, 43–80.
28 C.-Y. Su, B.-S. Kang, C.-X. Du, Q.-C. Yang and T. C. Mak, *Inorg. Chem.*, 2000, **39**, 4843–4849.
29 (*a*) C. Janiak, *J. Chem. Soc., Dalton Trans.*, 2000, 3885–3896; (*b*) A. N. Khlobystov, A. J. Blake, N. R. Champness, D. A. Lemenovskii, A. G. Majouga, N. V. Zyk and M. Schröder, *Coord. Chem. Rev.*, 2001, **222**, 155–192; (*c*) A. J. Blake, G. Baum, N. R. Champness, S. S. Chung, P. A. Cooke, D. Fenske, A. N. Khlobystov, D. A. Lemenovskii, W.-S. Li and M. Schröder, *J. Chem. Soc., Dalton Trans.*, 2000, 4285–4291; (*d*) C. A. Hunter and J. K. M. Sanders, *J. Am. Chem. Soc.*, 1990, **112**, 5525–5534.
30 F. van Bolhuis and C. T. Kiers, *Acta Crystallogr., Sect. B: Struct. Crystallogr. Cryst. Chem.*, 1978, **34**, 1015–1016.
31 J. Wang, S. G. Bodige, W. H. Watson and C. D. Gutsche, *J. Org. Chem.*, 2000, **65**, 8260–8263.
32 G. M. Sheldrick, *SHELXTL, 5.1 for Window NT, Structure Determination Software*, Bruker Analytical X-Ray Systems, Inc., Madison, Wisconsin, USA, 1997.

